AIMS Mathematics, 10(9): 20947–20978.
DOI: 10.3934/math.2025936
Received: 27 July 2025
Revised: 25 August 2025
Accepted: 29 August 2025
Published: 12 September 2025

http://www.aimspress.com/journal/Math

Research article

Optimal control of pandemic dynamics using a piecewise fractional order SVIR model

F. Gassem[1], Ashraf A. Qurtam[2], Mesfer H. Alqahtani[3], Mohammed Rabih[4,*], Khaled Aldwoah[5], Abdelaziz El-Sayed[6,*] and S. O. Ali[7]

[1] Department of Mathematics, College of Science, University of Ha'il, Ha'il 55473, Saudi Arabia
[2] Biology Department, College of Science, Imam Mohammad Ibn Saud Islamic University (IMSIU), Riyadh 11432, Saudi Arabia
[3] Department of Mathematics, University College of Umluj, University of Tabuk, Tabuk 48322, Saudi Arabia
[4] Department of Mathematics, College of Science, Qassim University, Buraydah 51452, Saudi Arabia
[5] Department of Mathematics, Faculty of Science, Islamic University of Madinah, Madinah 42351, Saudi Arabia
[6] Biology Department, Faculty of Science, Islamic University of Madinah, Madinah, Saudi Arabia
[7] Department of Mathematics and Statistics, Imam Mohammad Ibn Saud Islamic University (IMSIU), Riyadh 11432, Saudi Arabia

* **Correspondence:** Email: m.fadlallah@qu.edu.sa, aldwoah@iu.edu.sa.

Abstract: Modeling the long-term dynamics of the COVID-19 pandemic is challenged by evolving public behavior and interventions. We propose a novel piecewise fractional-order (SVIR) model incorporating vaccination and education controls. The model uniquely employs a classical derivative for the initial, memoryless phase of the epidemic. It then transitions to a Caputo-Fabrizio fractional derivative to capture long-term collective memory effects on transmission. We establish the model's mathematical well-posedness and derive the basic reproduction number (R_0). Under our baseline parameterization, the reproduction number is $R_0 \simeq 4.95$. An optimal control problem is formulated to determine the ideal implementation of time-varying vaccination and education. Numerical simulations validate the distinct crossover dynamics produced by our piecewise approach. Results demonstrate that a synergistic strategy combining vaccination and education is highly effective, reducing the peak of infected individuals by over 90% compared to the uncontrolled scenario, and significantly outperforms isolated interventions. This study offers a flexible tool for understanding and controlling epidemics.

Keywords: COVID-19 model; piecewise Caputo-Fabrizio model; basic reproduction number; optimal control; stability; simulation

Mathematics Subject Classification: 26A33, 34A08, 34A12

1. Introduction

Mathematical modeling has become an indispensable tool in epidemiology, providing critical insights into the transmission dynamics of infectious diseases and helping to evaluate the potential impact of public health interventions [1–3]. Foundational to this field are compartmental models, such as the susceptible-infected-recovered (SIR) framework and its derivatives, which have been instrumental in forecasting the trajectory of outbreaks like the COVID-19 pandemic [4–6]. These traditional models rely on integer-order differential equations, which operate under the assumption that the rate of change within a population depends solely on the current state of the system. However, this "memoryless" property, while mathematically convenient, often fails to capture the complexity of human behavior over the course of a protracted pandemic.

During a global event like COVID-19, population behavior is not static; it evolves. Sustained public awareness, media saturation, personal experiences with the disease, and official health messaging create a "collective memory" that influences long-term behavioral patterns such as mask-wearing, social distancing, and vaccine uptake. To address the limitations of memoryless models, researchers have increasingly turned to fractional calculus. Fractional-order derivatives, such as those developed by Riemann [7], Hadamard [8], Caputo [9], Atangana-Baleanu [10], and Caputo-Fabrizio [11], are inherently non-local due to their integral definitions. This property allows them to capture historical information, making them uniquely suited to model systems with memory effects and providing more nuanced descriptions of epidemic dynamics [12–14]. The versatility of fractional operators has led to their application across a wide range of scientific domains. In epidemiology, for instance, researchers have effectively used the Atangana-Baleanu-Caputo (ABC) operator to create extended SEIR models for COVID-19, providing deeper insights into its transmission dynamics [15]. Beyond epidemiology, these advanced mathematical tools are used to investigate the Hyers-Ulam stability of complex systems like computer virus models [16]. Furthermore, modern approaches have begun to merge fractional calculus with machine learning, combining Caputo derivatives with artificial neural networks to create powerful predictive models for other viral diseases like Hepatitis B [17]. Methodologies like the Laplace-Adomian decomposition method have been successfully used to identify and analyze chaos in other fractional-order biological models, such as the glucose-insulin system [18], and the control of chaos in such systems [19].

A key application of these advanced modeling techniques is the integration of behavioral dynamics. A nuanced understanding of how factors like public caution and a perceived sense of safety impact transmission is essential for policymakers to design and implement targeted, effective mitigation strategies [20–22]. The importance of quantifying human behavior is well-documented, with researchers like Funk et al. [23] and Verelst et al. [24] exploring both the challenges and opportunities in this area. Building on this foundation, Forrest and Al-arydah [25] recently proposed an integer-order SVIR model that defines the transmission rate as an exponential function of the infected population, crucially distinguishing between vaccinated and unvaccinated individuals. Their work provides a robust framework for analyzing the interplay between public behavior and optimal

control in a standard ODE setting.

However, their integer-order approach, like other classical models, is inherently memoryless. This presents a conceptual challenge: the initial outbreak is often characterized by panic and rapid, reactive changes, a dynamic better captured by the memoryless nature of classical derivatives. In contrast, imposing a memory effect from day one may not accurately reflect the initial social response. A single framework, whether purely integer-order or purely fractional-order, is therefore insufficient to capture the transition from an early-stage, reactive response to a long-term, memory-informed "new normal." To the best of our knowledge, no existing model combines piecewise derivatives to capture the transition in behavioral memory effects with a comprehensive optimal control analysis for pandemic management.

To address this critical gap, this study generalizes the model structure proposed by Forrest and Al-arydah [25] by implementing a novel piecewise fractional-order derivative. We adopt their five-compartment SVIR framework and behavioral transmission function but replace the classical derivative with a piecewise operator that transitions from a classical integer-order derivative for the initial phase, $[0, \varsigma_1]$, to a Caputo-Fabrizio (CF) fractional derivative for the subsequent, long-term phase, $(\varsigma_1, T]$. The choice of the Caputo-Fabrizio operator is deliberate. Its non-singular exponential kernel implies an exponentially fading memory, which we hypothesize is more biologically plausible for long-term behavioral changes than the power-law memory implied by singular kernels or the Mittag-Leffler kernel of the Atangana-Baleanu derivative. The exponential decay represents a gradual return to normalcy, where the immediate past is more influential than the distant past. This hybrid approach is the core of our study, allowing us to investigate how the introduction of memory effects alters the epidemic dynamics and optimal control strategies originally explored in a memoryless context. The primary contributions of this work are therefore fourfold:

- Novel Model Formulation: We propose and formulate a novel piecewise fractional-order SVIR model that extends a recent integer-order framework. Its unique structure, which distinguishes between population subgroups and, most critically, utilizes a piecewise operator to transition from memoryless to memory-informed dynamics, offers a more realistic framework than the single-paradigm models used in previous research.
- Rigorous Mathematical Analysis: We establish the fundamental properties of the model, including the positivity and boundedness of solutions. We derive the basic reproduction number ($\mathbb{R}_0$) as a critical threshold for disease invasion and analyze the local stability of the disease-free equilibrium.
- Comprehensive Optimal Control Design: We design an optimal control problem incorporating two key real-world interventions: a time-varying vaccination effort and a public education campaign to reduce transmission. We solve for the optimal control strategies using Pontryagin's Maximum Principle.
- Synergistic Intervention and Realistic Simulation: Through extensive numerical simulations with biologically plausible parameters, we demonstrate the powerful synergistic effect of combining vaccination and education, showing it vastly outperforms either intervention alone. Crucially, we validate that our piecewise framework produces more realistic long-term epidemic dynamics compared to classical models.

This framework offers a flexible and realistic tool for understanding and controlling epidemics

characterized by shifting population dynamics and providing critical insights into the optimal deployment of control measures.

The structure of the remaining sections is as follows: In Section 2, we first introduce the mathematical framework, presenting a five-compartment SVIR-type model that distinguishes between vaccinated and unvaccinated populations, and we rigorously establish its fundamental properties by proving the positivity and boundedness of its solutions. Following this, in Sections 3 and 4, we analyze the model's intrinsic dynamics by identifying the disease-free equilibrium and deriving the crucial basic reproduction number ($\mathbb{R}_0$), which defines the epidemic threshold, complemented by a local stability analysis that formally proves the conditions for disease invasion. To bridge theory with application, Section 5 investigates the model's sensitivity to key parameters and then formulates an optimal control problem designed to minimize infections and intervention costs through time-varying vaccination and public education strategies. Finally, after detailing the numerical scheme in Section 6, the core findings are presented in Section 7. There, extensive simulations first establish a catastrophic baseline epidemic. The results then demonstrate that the combined synergistic effect of vaccination and education provides a profoundly more effective suppression of the disease than any single intervention alone, thus validating our theoretical framework and providing strong quantitative support for multi-faceted public health policies.

2. Mathematical model

We present a piecewise fractional-order epidemiological model whose underlying integer-order structure is based on the SVIR framework developed by Forrest and Al-arydah [25]. The total population $N(\varsigma)$ is divided into five compartments: susceptibles $S(\varsigma)$, vaccinated $V(\varsigma)$, infected vaccinated $I_v(\varsigma)$, infected unvaccinated $I_u(\varsigma)$, and recovered $R(\varsigma)$. In modeling the behavioral response to the pandemic, the time-dependent transmission rate $\beta(\varsigma)$ can be viewed as a product of the baseline transmission rate β_0 and functions representing public caution and sense of safety. A comprehensive formulation is often given by $\beta(I, V) = \beta_0 f_I f_V$ [26], where f_I models the reduction in transmission due to caution from rising infections and f_V models a potential increase in transmission due to a relaxed sense of safety from vaccination.

For the scope of this particular study, we focus primarily on the effect of caution driven by active case counts. We therefore make the simplifying assumption that the population's sense of safety is not significantly impacted by the vaccination level, setting $f_V = 1$. This leads to the transmission rate $\beta(I)$ used in our model, which depends only on the number of infected individuals. Acknowledging this is a simplification, we leave the exploration of post-vaccination behavioral relaxation for future work. The model includes a constant recruitment rate Π, a natural per capita death rate μ, and a time-dependent vaccination control effort $u(\varsigma)$, which results in a vaccination rate of $\alpha u(\varsigma)S(\varsigma)$. The force of infection, λ, is given by

$$\lambda(\varsigma) = \frac{\beta(I)\,(I_u(\varsigma) + \eta I_v(\varsigma))}{N(\varsigma)},$$

where the transmission rate $\beta(I)$ depends on the total number of infected individuals $I(\varsigma) = I_u(\varsigma) + I_v(\varsigma)$ to model behavioral changes:

$$\beta(I) = \beta_0 e^{-d_I I}.$$

The model of piecewise fractional-order differential equations is:

$$\begin{cases} {}^{PC-F}\mathbf{D}_{\varsigma}^{\delta} S\left(\varsigma\right) = \Pi - \left(\frac{\beta_0 e^{-d_I I}(I_u+\eta I_v)}{N} + \alpha u + \mu\right) S\left(\varsigma\right), \\ {}^{PC-F}\mathbf{D}_{\varsigma}^{\delta} V\left(\varsigma\right) = \alpha u S\left(\varsigma\right) - \left(\frac{\beta_0 e^{-d_I I}(I_u+\eta I_v)}{N}\epsilon + \mu\right) V(\varsigma), \\ {}^{PC-F}\mathbf{D}_{\varsigma}^{\delta} I_v\left(\varsigma\right) = \frac{\beta_0 e^{-d_I I}(I_u+\eta I_v)}{N}\epsilon V(\varsigma) - (\gamma_v + \mu + \rho_v) I_v\left(\varsigma\right), \\ {}^{PC-F}\mathbf{D}_{\varsigma}^{\delta} I_u\left(\varsigma\right) = \frac{\beta_0 e^{-d_I I}(I_u+\eta I_v)}{N} S\left(\varsigma\right) - (\gamma_u + \mu + \rho_u) I_u\left(\varsigma\right), \\ {}^{PC-F}\mathbf{D}_{\varsigma}^{\delta} R\left(\varsigma\right) = \gamma_v I_v(\varsigma) + \gamma_u I_u(\varsigma) - \mu R\left(\varsigma\right), \end{cases} \tag{2.1}$$

with the general initial conditions: $S\left(0\right) > 0, V\left(0\right) > 0, I_v\left(0\right) > 0, I_u\left(0\right) > 0, R\left(0\right) > 0$. Here, the operator ${}^{PC-F}\mathbf{D}_{\varsigma}^{\delta}$ represents the piecewise Caputo-Fabrizio derivative. The transition point, ς_1, is a critical parameter representing the time at which the epidemic dynamics shift from being memoryless to being influenced by memory effects. The choice of ς_1 can be motivated by significant real-world events, such as the end of an initial strict lockdown, the rollout of a major public health education campaign, or the point where vaccination becomes widely available. In the context of this theoretical study, ς_1 is treated as a parameter that defines the duration of the initial reactive phase. The formal definition of the piecewise operator [11] used in system (2.1) ensures continuity of the state variables at ς_1 and is given by:

$${}^{PC-F}\mathbf{D}_{\varsigma}^{\delta} G\left(\varsigma\right) = \begin{cases} \frac{d}{d\varsigma} G\left(\varsigma\right), \varsigma \in [0, \varsigma_1], \\ {}^{C-F}\mathbf{D}_{\varsigma}^{\delta} G\left(\varsigma\right), \varsigma \in (\varsigma_1, T], \end{cases} \tag{2.2}$$

where $\frac{d}{d\varsigma} G\left(\varsigma\right)$ is the classical derivative, and ${}^{C-F}\mathbf{D}_{\varsigma}^{\delta} G\left(\varsigma\right)$ is the Caputo-Fabrizio fractional derivative. The operator is defined such that the memory kernel of the CF derivative integrates from the switching point ς_1, not from 0, ensuring the system's history before ς_1 influences the state at ς_1 but not the subsequent memory dynamics directly. The well-posedness of such hybrid systems across the interface is established through theorems that guarantee existence and uniqueness, provided the system's right-hand side satisfies Lipschitz conditions in each sub-interval. The corresponding piecewise integral is given by:

$$G(\varsigma) = \begin{cases} G(0) + \int_0^{\varsigma} F(s, G(s)) ds, \quad \varsigma \in [0, \varsigma_1], \\ G(\varsigma_1) + \frac{1-\delta}{\Delta(\delta)} F(\varsigma, G(\varsigma)) + \frac{\delta}{\Delta(\delta)} \int_{\varsigma_1}^{\varsigma} F(s, G(s)) ds, \quad \varsigma \in (\varsigma_1, T], \end{cases} \tag{2.3}$$

where $\Delta(\delta)$ is a normalization function. Epidemiologically, ς_1 can be identified as the time corresponding to a major shift in public policy or behavior, such as the end of a lockdown or the start of a mass vaccination campaign. Statistically, ς_1 could be estimated from epidemiological time-series data by identifying a structural break point where the decay dynamics of infections change. The Schematic diagram of the piecewise fractional-order SVIR model (2.1) is presented in Figure 1.

The parameter values listed in Table 1 are chosen to represent a biologically plausible scenario for a COVID-19-like epidemic and are adapted from the baseline parameters used in the foundational integer-order model by Forrest and Al-arydah [25]. This ensures that our exploration of memory effects is directly comparable to their original memoryless framework. Minor adjustments were made to certain parameters to better highlight the specific dynamics of the piecewise system. It is important

to emphasize that this study is theoretical; therefore, the parameters were not re-calibrated against a new dataset but were selected to generate a significant baseline epidemic ($R_0 \approx 4.95$) against which the impact of memory and optimal control could be clearly demonstrated.

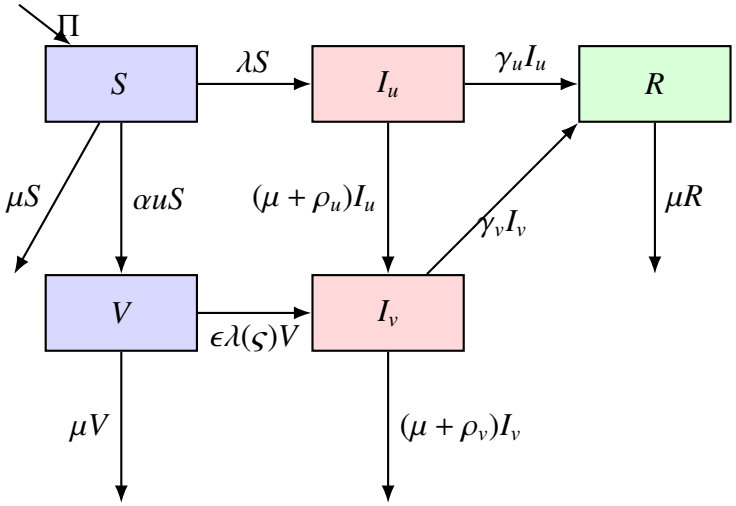

Figure 1. Schematic diagram of the piecewise fractional-order SVIR model.

Table 1. Model parameter definitions and their values.

Parameter	Description	Value	Unit
Π	Recruitment rate	29.4	persons day^{-1}
α	Maximum vaccination rate coefficient	0.1	day^{-1}
β_0	Baseline transmission rate	0.25	day^{-1}
d_I	Sense of caution factor	20	person^{-1}
η	Relative infectivity of vaccinated individuals	0.5	dimensionless
μ	Natural mortality rate	3.4×10^{-5}	day^{-1}
ϵ	Relative susceptibility of vaccinated	0.2	dimensionless
γ_v	Recovery rate of infected vaccinated	$\frac{1}{14}$	day^{-1}
γ_u	Recovery rate of infected unvaccinated	$\frac{1}{20}$	day^{-1}
ρ_v	Disease-induced death rate (vaccinated)	0.00005	day^{-1}
ρ_u	Disease-induced death rate (unvaccinated)	0.0005	day^{-1}

3. Properties of the model

3.1. Positivity of solutions

To show that the solutions remain non-negative, we examine the behavior of the model on the boundaries of the non-negative orthant $\mathbb{R}^5_+$. By the first equation in model 2.1, we have

$$^{PC-F}\mathbf{D}^{\delta}_{\varsigma} S\,(\varsigma) = \Pi - \left(\frac{\beta_0 e^{-d_I I}\,(I_u + \eta I_v)}{N} + \alpha u + \mu\right) S\,(\varsigma) \geq -\left(\frac{\beta_0 e^{-d_I I}\,(I_u + \eta I_v)}{N} + \alpha u + \mu\right) S\,(\varsigma). \quad (3.1)$$

This result intuitively means that if $S(\varsigma)$ were to become zero, its rate of change would be $\Pi \geq 0$, preventing it from becoming negative. A more formal proof follows. By definition of piecewise Caputo-Fabrizio fractional derivative 2.2, we can rewrite Eq (3.1) as follows:

$$\begin{cases} \frac{d}{d\varsigma} S(\varsigma) \geq -\left(\frac{\beta_0 e^{-d_I I}(I_u+\eta I_v)}{N} + \alpha u + \mu\right) S(\varsigma), \varsigma \in [0, \varsigma_1], \\ {}^{C-F}\mathbf{D}_{\varsigma}^{\delta} S(\varsigma) \geq -\left(\frac{\beta_0 e^{-d_I I}(I_u+\eta I_v)}{N} + \alpha u + \mu\right) S(\varsigma), \varsigma \in (\varsigma_1, T]. \end{cases}$$

In the case $\varsigma \in [0, \varsigma_1]$, we have

$$S(\varsigma) \geq S(0) \exp\left(-\int_0^{\varsigma} \left(\frac{\beta_0 e^{-d_I I}(I_u + \eta I_v)}{N} + \alpha u + \mu\right) d\varrho > 0. \tag{3.2}$$

In the case $\varsigma \in (\varsigma_1, T]$, we have

$${}^{C-F}\mathbf{D}_{\varsigma}^{\delta} S(\varsigma) \geq -\left(\frac{\beta_0 e^{-d_I I}(I_u + \eta I_v)}{N} + \alpha u + \mu\right) S(\varsigma). \tag{3.3}$$

To prove positivity on the interval $(\varsigma_1, T]$, we provide a detailed argument using the Laplace transform, specifically addressing the piecewise nature of the system. Let us define a new time variable $\tau = \varsigma - \varsigma_1$ such that the interval begins at $\tau = 0$. The governing inequality for $S(\tau)$ is then:

$${}^{C-F}\mathbf{D}_{\tau}^{\delta} S(\tau) \geq -CS(\tau), \quad \text{with initial condition } S(\tau = 0) = S(\varsigma_1),$$

where $C = \left(\frac{\beta_0 e^{-d_I I}(I_u+\eta I_v)}{N} + \alpha u + \mu\right)$ is a positive, time-dependent coefficient that we can consider constant for this local analysis. Rearranging, we have ${}^{C-F}\mathbf{D}_{\tau}^{\delta} S(\tau) + CS(\tau) = g(\tau)$, where $g(\tau) \geq 0$.

We now apply the Laplace transform $\mathcal{L}\{\cdot\}$ with respect to τ. Using the known transform for the Caputo-Fabrizio derivative, $\mathcal{L}\{{}^{C-F}\mathbf{D}_{\tau}^{\delta} f(\tau)\} = \frac{p\bar{f}(p) - f(0)}{(1-\delta)p + \delta}$, we get:

$$\frac{p\bar{S}(p) - S(\varsigma_1)}{(1-\delta)p + \delta} + C\bar{S}(p) = \bar{g}(p),$$

where $\bar{S}(p)$ and $\bar{g}(p)$ are the Laplace transforms of $S(\tau)$ and $g(\tau)$, respectively. Solving for $\bar{S}(p)$ yields:

$$\bar{S}(p) = \frac{S(\varsigma_1)}{p(1 + C(1-\delta)) + C\delta} + \frac{((1-\delta)p + \delta)\bar{g}(p)}{p(1 + C(1-\delta)) + C\delta}.$$

To find $S(\tau)$, we take the inverse Laplace transform.

(1) The first term has the form of a simple exponential decay, $\mathcal{L}^{-1}\left\{\frac{A}{p+B}\right\} = Ae^{-B\tau}$, which is always non-negative since $S(\varsigma_1) > 0$ from the first interval's solution.
(2) For the second term, we know that since $g(\tau) \geq 0$, its transform $\bar{g}(p)$ is non-negative for real p. The entire second term is a product of transforms whose inverses are non-negative. The inverse transform is therefore a convolution of two non-negative functions, which is itself non-negative.

Since $S(\tau)$ is the sum of two non-negative functions, we conclude that $S(\tau) \geq 0$. This holds for all $\tau > 0$, which means $S(\varsigma) \geq 0$ for all $\varsigma \in (\varsigma_1, T]$.

3.2. Boundedness of solutions

The total population $N(\varsigma) = S(\varsigma)+V(\varsigma)+I_v(\varsigma)+I_u(\varsigma)+R(\varsigma)$. Summing the equations in system (2.1):

$$\begin{aligned} {}^{PC-F}\mathbf{D}_{\varsigma}^{\delta}N(\varsigma) &= {}^{PC-F}\mathbf{D}_{\varsigma}^{\delta}S(\varsigma) + {}^{PC-F}\mathbf{D}_{\varsigma}^{\delta}V(\varsigma) + {}^{PC-F}\mathbf{D}_{\varsigma}^{\delta}I_v(\varsigma) + {}^{PC-F}\mathbf{D}_{\varsigma}^{\delta}I_u(\varsigma) + {}^{PC-F}\mathbf{D}_{\varsigma}^{\delta}R(\varsigma) \\ &= \Pi - \mu N(\varsigma) - \rho_v I_v(\varsigma) - \rho_u I_u(\varsigma). \end{aligned}$$

Since $\rho_v I_v \geq 0$ and $\rho_u I_u \geq 0$, we have

$$ {}^{PC-F}\mathbf{D}_{\varsigma}^{\delta}N(\varsigma) \leq \Pi - \mu N(\varsigma). \tag{3.4}$$

This shows that if the total population $N(\varsigma)$ exceeds the equilibrium level Π/μ, its rate of change becomes negative, pulling it back toward the equilibrium. This ensures the solution remains bounded. By definition of piecewise Caputo-Fabrizio fractional derivative 2.2, we can rewrite Eq (3.4) as follows:

$$\begin{cases} \frac{d}{d\varsigma}N(\varsigma) \leq \Pi - \mu N(\varsigma), \varsigma \in [0, \varsigma_1], \\ {}^{C-F}\mathbf{D}_{\varsigma}^{\delta}N(\varsigma) \leq \Pi - \mu N(\varsigma), \varsigma \in (\varsigma_1, T]. \end{cases}$$

In the first case $\varsigma \in [0, \varsigma_1]$, we get

$$N(\varsigma) \leq N(0)e^{-\mu\varsigma} + \frac{\Pi}{\mu}(1 - e^{-\mu\varsigma}).$$

Thus $N(\varsigma)$ is bounded by $\max(N(0), \frac{\Pi}{\mu})$, for all $\varsigma \in [0, \varsigma_1]$. In the second case $\varsigma \in (\varsigma_1, T]$, by applying comparison theorems for fractional differential equations, we can show that $N(\varsigma)$ is bounded by the solution to the corresponding equality. If $N(\varsigma_1) \leq \frac{\Pi}{\mu}$, then $N(\varsigma) \leq \frac{\Pi}{\mu}$ for all $\varsigma > \varsigma_1$. If $N(\varsigma_1) > \frac{\Pi}{\mu}$, then $N(\varsigma)$ will eventually approach $\frac{\Pi}{\mu}$. Thus, the total population $N(\varsigma)$ is bounded. Since all individual populations are non-negative, they are also bounded. The feasible region Ω is a positively invariant set for system (2.1), where

$$\Omega = \left\{(S, V, I_v, I_u, R) \in \mathbb{R}_+^5 : S + V + I_v + I_u + R \leq \max\left(N(0), \frac{\Pi}{\mu}\right)\right\}.$$

3.3. Existence and uniqueness

For non-negative initial conditions, a unique solution to the model 2.1 exists in $\mathbb{R}_+^5$. This can be established by showing that the function on the right-hand side of the system is locally Lipschitz continuous with respect to the state variables. Given that the state variables are bounded within the feasible region Ω, the non-linear incidence term $\beta_0 e^{-d_I I}$ and its derivatives are also bounded, which ensures the Lipschitz condition holds. For the piecewise operator, existence and uniqueness are guaranteed in each sub-interval, and continuity at the transition point ς_1 ensures a well-posed solution over the entire domain $[0, T]$.

Theorem 3.1 (Existence and uniqueness)**.** *The piecewise fractional-order system* (2.1) *has a unique solution* $G(\varsigma) \in C([0, T], \mathbb{R}^5)$ *for any given initial condition* $G(0)$ *in the feasible region* Ω*.*

Proof. The proof is based on the Banach fixed-point Theorem. The system can be expressed in its equivalent piecewise integral form. We define a single operator $\mathcal{T}$ on the Banach space $C([0, T], \mathbb{R}^5)$

(the space of continuous functions from $[0, T]$ to $\mathbb{R}^5$) equipped with the supremum norm $\|\cdot\|_\infty$. For any $G \in C([0, T], \mathbb{R}^5)$, the operator $\mathcal{T}$ is defined as:

$$(\mathcal{T}G)(\varsigma) = \begin{cases} G(0) + \int_0^\varsigma \mathcal{F}(s, G(s))ds, & \varsigma \in [0, \varsigma_1] \\ (\mathcal{T}G)(\varsigma_1) + \frac{1-\delta}{\Delta(\delta)}\mathcal{F}(\varsigma, G(\varsigma)) + \frac{\delta}{\Delta(\delta)}\int_{\varsigma_1}^\varsigma \mathcal{F}(s, G(s))ds, & \varsigma \in (\varsigma_1, T], \end{cases}$$

where $G(\varsigma) = (S(\varsigma), V(\varsigma), I_v(\varsigma), I_v(\varsigma), R(\varsigma))^T$, and

$$F(\varsigma, G(\varsigma)) = \begin{cases} F_1(\varsigma, S(\varsigma), V(\varsigma), I_v(\varsigma), I_u(\varsigma), R(\varsigma)) = \Pi - \left(\frac{\beta_0 e^{-d_I I}(I_u + \eta I_v)}{N} + \alpha u + \mu\right) S(\varsigma), \\ F_2(\varsigma, S(\varsigma), V(\varsigma), I_v(\varsigma), I_u(\varsigma), R(\varsigma)) = \alpha u S(\varsigma) - \left(\frac{\beta_0 e^{-d_I I}(I_u + \eta I_v)}{N}\epsilon + \mu\right) V(\varsigma), \\ F_3(\varsigma, S(\varsigma), V(\varsigma), I_v(\varsigma), I_u(\varsigma), R(\varsigma)) = \frac{\beta_0 e^{-d_I I}(I_u + \eta I_v)}{N}\epsilon V(\varsigma) - (\gamma_v + \mu + \rho_v) I_v(\varsigma), \\ F_4(\varsigma, S(\varsigma), V(\varsigma), I_v(\varsigma), I_u(\varsigma), R(\varsigma)) = \frac{\beta_0 e^{-d_I I}(I_u + \eta I_v)}{N} S(\varsigma) - (\gamma_u + \mu + \rho_u) I_u(\varsigma), \\ F_5(\varsigma, S(\varsigma), V(\varsigma), I_v(\varsigma), I_u(\varsigma), R(\varsigma)) = \gamma_v I_v(\varsigma) + \gamma_u I_u(\varsigma) - \mu R(\varsigma). \end{cases}$$

The vector $\mathcal{F}$ is Lipschitz continuous with respect to its second argument (constant $L_{\mathcal{F}}$) within the bounded region Ω. The operator is constructed to be continuous at ς_1 by using the value $(\mathcal{T}G)(\varsigma_1)$ from the first definition as the starting point for the second. A solution to the system is a fixed point of $\mathcal{T}$.

We now show that $\mathcal{T}$ is a contraction mapping. Let $G_1, G_2 \in C([0, T], \mathbb{R}^5)$.

For $\varsigma \in [0, \varsigma_1]$:

$$\begin{aligned} \|(\mathcal{T}G_1)(\varsigma) - (\mathcal{T}G_2)(\varsigma)\| &\le \int_0^\varsigma \|\mathcal{F}(s, G_1(s)) - \mathcal{F}(s, G_2(s))\|ds \\ &\le L_{\mathcal{F}} \int_0^\varsigma \|G_1(s) - G_2(s)\|ds \le L_{\mathcal{F}}\varsigma_1 \|G_1 - G_2\|_\infty. \end{aligned}$$

For $\varsigma \in (\varsigma_1, T]$:

$$\begin{aligned} \|(\mathcal{T}G_1)(\varsigma) - (\mathcal{T}G_2)(\varsigma)\| &\le \|(\mathcal{T}G_1)(\varsigma_1) - (\mathcal{T}G_2)(\varsigma_1)\| \\ &\quad + \frac{1-\delta}{\Delta(\delta)}\|\mathcal{F}(\varsigma, G_1) - \mathcal{F}(\varsigma, G_2)\| + \frac{\delta}{\Delta(\delta)}\int_{\varsigma_1}^\varsigma \|\mathcal{F}(s, G_1) - \mathcal{F}(s, G_2)\|ds \\ &\le L_{\mathcal{F}}\varsigma_1 \|G_1 - G_2\|_\infty + \frac{L_{\mathcal{F}}}{\Delta(\delta)}(1-\delta)\|G_1 - G_2\|_\infty \\ &\quad + \frac{L_{\mathcal{F}}\delta}{\Delta(\delta)}(T - \varsigma_1)\|G_1 - G_2\|_\infty \\ &\le \left(L_{\mathcal{F}}\varsigma_1 + \frac{L_{\mathcal{F}}}{\Delta(\delta)}\left[1 - \delta + \delta(T - \varsigma_1)\right]\right)\|G_1 - G_2\|_\infty. \end{aligned}$$

Let $\Theta = L_{\mathcal{F}} \max\left\{\varsigma_1,\ \varsigma_1 + \frac{1-\delta+\delta(T-\varsigma_1)}{\Delta(\delta)}\right\}$. Then, taking the supremum over the entire interval $[0, T]$, we get:

$$\|\mathcal{T}G_1 - \mathcal{T}G_2\|_\infty \le \Theta\|G_1 - G_2\|_\infty.$$

By choosing a sufficiently small time horizon T (and thus $\varsigma_1 < T$), we can ensure that $\Theta < 1$. For any arbitrary time horizon, the proof can be applied over successive small intervals. Therefore, $\mathcal{T}$ is a contraction mapping. By the Banach fixed-point Theorem, $\mathcal{T}$ has a unique fixed point, which corresponds to the unique solution of the system on $[0, T]$. □

4. Equilibrium analysis (without time-dependent optimal control)

For this section, we consider the model without active time-varying optimal controls. For the DFE, we assume $u = 0$.

4.1. Disease-free equilibrium (DFE)

The DFE, denoted $E_0 = (S^0, V^0, I_v^0, I_u^0, R^0)$, is obtained by setting $I_v = I_u = 0$. This implies $\lambda(0) = 0$. We also assume no control, so $u = 0$. The system at steady state becomes:

$$\begin{aligned}
0 &= \Pi - \mu S^0 \implies S^0 = \frac{\Pi}{\mu} \\
0 &= -\mu V^0 \implies V^0 = 0 \\
0 &= -(\gamma_v + \mu + \rho_v) I_v^0 \implies I_v^0 = 0 \\
0 &= -(\gamma_u + \mu + \rho_u) I_u^0 \implies I_u^0 = 0 \\
0 &= -\mu R^0 \implies R^0 = 0
\end{aligned}$$

So, the DFE is $E_0 = (\frac{\Pi}{\mu}, 0, 0, 0, 0)$. At DFE, $N^0 = S^0 = \frac{\Pi}{\mu}$.

4.2. Basic reproduction number (R_0)

We use the next-generation matrix method. The infected compartments are I_v and I_u. Let $x = (I_v, I_u)^T$. The new infections terms are $\mathcal{F}_i$ and transfer terms are $\mathcal{V}_i$.

$$^{PC-F}\mathbf{D}_{\varsigma}^{\delta} I_v = \frac{\beta_0 e^{-d_I I}\,(I_u + \eta I_v)}{N} \epsilon V(\varsigma) - (\gamma_v + \mu + \rho_v) I_v(\varsigma),$$

$$^{PC-F}\mathbf{D}_{\varsigma}^{\delta} I_u(\varsigma) = \frac{\beta_0 e^{-d_I I}\,(I_u + \eta I_v)}{N} S(\varsigma) - (\gamma_u + \mu + \rho_u) I_u(\varsigma).$$

It is important to state prominently that the following derivation of R_0 assumes that the system is at the disease-free equilibrium where the vaccinated compartment is empty ($V_0 = 0$). The new infections matrix F and transition matrix V_m evaluated at E_0 are given as follows:

$$F = \begin{pmatrix} 0 & 0 \\ \beta_0\eta & \beta_0 \end{pmatrix} \quad \text{and} \quad V_m = \begin{pmatrix} k_v & 0 \\ 0 & k_u \end{pmatrix},$$

and

$$V_m^{-1} = \begin{pmatrix} \frac{1}{k_v} & 0 \\ 0 & \frac{1}{k_u} \end{pmatrix},$$

where $k_v = \gamma_v + \mu + \rho_v$ and $k_u = \gamma_u + \mu + \rho_u$. The next-generation matrix is given as follows:

$$FV_m^{-1} = \begin{pmatrix} 0 & 0 \\ \frac{\beta_0\eta}{k_v} & \frac{\beta_0}{k_u} \end{pmatrix}.$$

The eigenvalues are 0 and $\frac{\beta_0}{k_u}$. Thus, the basic reproduction number is given as follows:

$$R_0 = \frac{\beta_0}{\gamma_u + \mu + \rho_u}.$$

This formulation of R_0 indicates that the initial spread is driven by unvaccinated individuals if there is no pre-existing vaccinated population. If there were a constant baseline vaccination leading to $V^0 > 0$, the derivation would be different, and the resulting R_0 would also depend on parameters like ϵ and η. However, for an emerging disease scenario, the assumption $V^0 = 0$ is standard. It is also important to note that the basic reproduction number, R_0, is independent of the fractional order δ. This is because R_0 is a threshold quantity determined by the initial growth rate of the epidemic from the disease-free equilibrium, which depends on the eigenvalues of the Jacobian matrix. While the value of δ critically affects the long-term dynamics and the conditions for asymptotic stability (as per Matignon's criterion), it does not alter this initial invasion threshold.

Alternative R_0 with baseline vaccination ($V^0 > 0$)

To address the scenario where a constant baseline vaccination strategy is in place, let us consider a constant control $u(\varsigma) = u_0$, where $0 < u_0 \leq 1$. In this case, the disease-free equilibrium (DFE) is different, as there will be a non-zero vaccinated population. By setting the infected compartments to zero ($I_v = I_u = 0$), the new DFE, denoted by $E_0^v = (S_v^0, V_v^0, 0, 0, 0)$, is found by solving:

$$\begin{aligned} 0 &= \Pi - (\alpha u_0 + \mu) S_v^0, \\ 0 &= \alpha u_0 S_v^0 - \mu V_v^0. \end{aligned}$$

This yields the DFE components:

$$S_v^0 = \frac{\Pi}{\alpha u_0 + \mu} \quad \text{and} \quad V_v^0 = \frac{\alpha u_0}{\mu} S_v^0 = \frac{\alpha u_0 \Pi}{\mu(\alpha u_0 + \mu)}.$$

The total population at this DFE is $N_v^0 = S_v^0 + V_v^0 = \frac{\Pi}{\mu}$.

To derive the basic reproduction number for this equilibrium, $R_{0,v}$, we again use the next-generation matrix method. The new infections matrix, F_v, and the transition matrix, V_m, are linearized around the new DFE, E_0^v. At this equilibrium, $I = 0$, so $\beta(I) = \beta_0$. The new infections matrix F_v is given by:

$$F_v = \begin{pmatrix} \frac{\beta_0 \epsilon V_v^0 \eta}{N_v^0} & \frac{\beta_0 \epsilon V_v^0}{N_v^0} \\ \frac{\beta_0 S_v^0 \eta}{N_v^0} & \frac{\beta_0 S_v^0}{N_v^0} \end{pmatrix} = \frac{\beta_0 \mu}{\Pi} \begin{pmatrix} \epsilon V_v^0 \eta & \epsilon V_v^0 \\ S_v^0 \eta & S_v^0 \end{pmatrix}.$$

The transition matrix V_m is unchanged: $V_m = \text{diag}(k_v, k_u)$. The next-generation matrix is $F_v V_m^{-1}$. The determinant of this matrix is zero, so one eigenvalue is 0. The other eigenvalue, which is the basic reproduction number, is equal to the trace of the matrix:

$$R_{0,v} = \rho(F_v V_m^{-1}) = \text{tr}(F_v V_m^{-1}) = \frac{\beta_0 \mu}{\Pi} \left(\frac{\epsilon V_v^0 \eta}{k_v} + \frac{S_v^0}{k_u} \right).$$

Substituting the expressions for S_v^0 and V_v^0:

$$R_{0,v} = \frac{\beta_0}{\alpha u_0 + \mu} \left(\frac{\alpha u_0 \epsilon \eta}{k_v} + \frac{\mu}{k_u} \right).$$

This expression for $R_{0,v}$ clearly shows that the epidemic threshold now depends on the baseline vaccination effort (u_0) and the vaccine's properties (ϵ, η). As u_0 increases, the denominator grows and the term multiplying μ/k_u shrinks, generally leading to a reduction in the reproduction number, which highlights the public health benefit of a persistent vaccination program.

4.3. Endemic equilibrium (EE)

The endemic equilibrium $E^{**} = (S^{**}, V^{**}, I_v^{**}, I_u^{**}, R^{**})$ is found by setting the right-hand sides of model (2.1) to zero, with $I_v^{**} > 0, I_u^{**} > 0$. This leads to a system of non-linear algebraic equations:

$$\begin{aligned}
\Pi &= \left(\frac{\beta_0 e^{-d_I I^{**}}(I_u^{**} + \eta I_v^{**})}{N^{**}} + \alpha u^{**} + \mu\right) S^{**}, \\
\alpha u^{**} S^{**} &= \left(\frac{\beta_0 e^{-d_I I^{**}}(I_u^{**} + \eta I_v^{**})}{N^{**}} \epsilon + \mu\right) V^{**}, \\
(\gamma_v + \mu + \rho_v) I_v^{**} &= \frac{\beta_0 e^{-d_I I^{**}}(I_u^{**} + \eta I_v^{**})}{N^{**}} \epsilon V^{**}, \\
(\gamma_u + \mu + \rho_u) I_u^{**} &= \frac{\beta_0 e^{-d_I I^{**}}(I_u^{**} + \eta I_v^{**})}{N^{**}} S^{**}, \\
\mu R^{**} &= \gamma_v I_v^{**} + \gamma_u I_u^{**},
\end{aligned}$$

where $I^{**} = I_u^{**} + I_v^{**}$. Solving this system analytically is generally intractable. The existence of an EE typically occurs when $R_0 > 1$.

5. Stability analysis

The stability of the equilibria is determined by the eigenvalues of the Jacobian matrix evaluated at the equilibrium. For fractional-order systems, an equilibrium is locally asymptotically stable if all eigenvalues λ_j satisfy $|\arg(\lambda_j)| > \delta\pi/2$ (Matignon's condition).

5.1. Local stability of the disease-free equilibrium (DFE)

To analyze the local stability of the DFE, we derive the explicit form of the Jacobian matrix evaluated at $E_0 = (\Pi/\mu, 0, 0, 0, 0)$.

First, we compute the necessary partial derivatives of the force of infection, $\lambda(\varsigma) = \frac{\beta_0 e^{-d_I I}(I_u + \eta I_v)}{N}$, evaluated at the DFE, where $I = 0$, $N = N^0 = \Pi/\mu$, and $\lambda = 0$:

$$\begin{aligned}
\left.\frac{\partial \lambda}{\partial I_u}\right|_{E_0} &= \frac{\beta_0}{N^0}(1) = \frac{\beta_0 \mu}{\Pi} \\
\left.\frac{\partial \lambda}{\partial I_v}\right|_{E_0} &= \frac{\beta_0}{N^0}(\eta) = \frac{\beta_0 \mu \eta}{\Pi} \\
\left.\frac{\partial \lambda}{\partial S}\right|_{E_0} &= -\left.\frac{\lambda}{N}\right|_{E_0} = 0 \\
\left.\frac{\partial \lambda}{\partial V}\right|_{E_0} &= -\left.\frac{\lambda}{N}\right|_{E_0} = 0
\end{aligned}$$

$$\left.\frac{\partial \lambda}{\partial R}\right|_{E_0} = -\left.\frac{\lambda}{N}\right|_{E_0} = 0.$$

The state equations are:

$$\begin{aligned} f_S &= \Pi - (\lambda + \alpha u + \mu)S \\ f_V &= \alpha u S - (\epsilon\lambda + \mu)V \\ f_{I_v} &= \epsilon\lambda V - k_{Iv} I_v \\ f_{I_u} &= \lambda S - k_{Iu} I_u \\ f_R &= \gamma_v I_v + \gamma_u I_u - \mu R \end{aligned}$$

where $k_{Iv} = \gamma_v + \mu + \rho_v$ and $k_{Iu} = \gamma_u + \mu + \rho_u$. The Jacobian matrix $J(E_0)$ is constructed by taking the partial derivatives of these functions and evaluating them at the DFE (where $S = S^0$, $V = I_v = I_u = R = 0$, and $u = 0$). The resulting fully simplified, explicit form is:

$$J(E_0) = \begin{pmatrix} -\mu & 0 & -S^0 \left.\frac{\partial \lambda}{\partial I_v}\right|_{E_0} & -S^0 \left.\frac{\partial \lambda}{\partial I_u}\right|_{E_0} & 0 \\ 0 & -\mu & 0 & 0 & 0 \\ 0 & 0 & -k_{Iv} & 0 & 0 \\ \left.\lambda\right|_{E_0} & 0 & S^0 \left.\frac{\partial \lambda}{\partial I_v}\right|_{E_0} & S^0 \left.\frac{\partial \lambda}{\partial I_u}\right|_{E_0} - k_{Iu} & 0 \\ 0 & 0 & \gamma_v & \gamma_u & -\mu \end{pmatrix}.$$

Substituting $S^0 = \Pi/\mu$ and the calculated partial derivatives:

$$J(E_0) = \begin{pmatrix} -\mu & 0 & -\beta_0\eta & -\beta_0 & 0 \\ 0 & -\mu & 0 & 0 & 0 \\ 0 & 0 & -k_{Iv} & 0 & 0 \\ 0 & 0 & \beta_0\eta & \beta_0 - k_{Iu} & 0 \\ 0 & 0 & \gamma_v & \gamma_u & -\mu \end{pmatrix}.$$

The eigenvalues are $\lambda_1 = \lambda_2 = \lambda_3 = -\mu$, $\lambda_4 = -k_{Iv} = -(\gamma_v + \mu + \rho_v)$, and $\lambda_5 = \beta_0 - k_{Iu} = \beta_0 - (\gamma_u + \mu + \rho_u)$. All eigenvalues are real. The role of the fractional order δ enters through Matignon's stability criterion, $|\arg(\lambda_j)| > \delta\pi/2$, which defines the boundaries of the stable region in the complex plane.

- **When** $R_0 < 1$, all eigenvalues are negative. Their argument is π. The stability condition becomes $\pi > \delta\pi/2$, which simplifies to $2 > \delta$. Since $\delta \in (0, 1]$, this condition is always satisfied. Therefore, if $R_0 < 1$, the DFE is locally asymptotically stable for any fractional order.
- **When** $R_0 > 1$, the eigenvalue $\lambda_5 = \beta_0 - k_{Iu}$ becomes positive. Its argument is 0. The stability condition becomes $0 > \delta\pi/2$, which is never satisfied for any $\delta > 0$. Therefore, if $R_0 > 1$, the DFE is unstable, regardless of the fractional order.

The stability condition $R_0 < 1$ defines a threshold that partitions the model's parameter space into regions of disease extinction and endemic persistence. This is visualized in Figure 2, which illustrates the stability regions of the DFE within a three-dimensional parameter space defined by the baseline transmission rate (β_0), the recovery rate (γ_u), and the natural mortality rate (μ). In each subplot, the parameter space is divided by the stability plane $\beta_0 = \gamma_u + \mu + \rho_u$ (shown in yellow). The volume

below this plane (green) represents the stable region ($R_0 < 1$), while the volume above (magenta) is the unstable region ($R_0 > 1$). The six panels show that as the disease-induced death rate, ρ_u, increases, the stable region expands. This illustrates that a more virulent disease removes individuals from the transmission cycle more quickly, making the epidemic less likely to be self-sustaining.

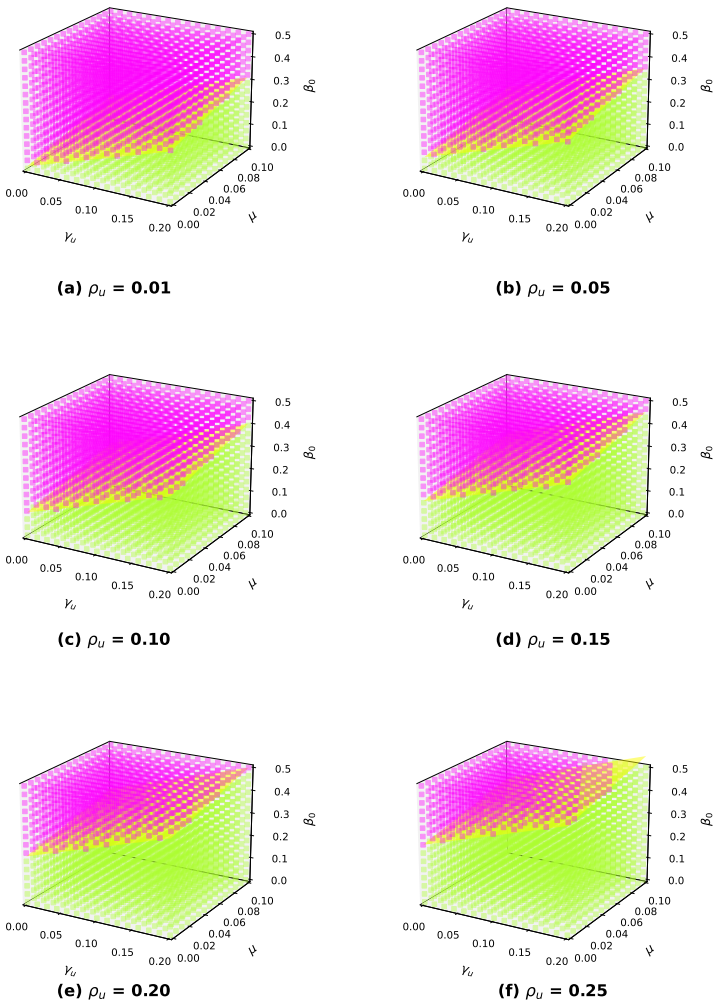

Figure 2. 3D visualization of the stability regions for the DFE. The stable region ($R_0 < 1$) is shown in green, while the unstable region ($R_0 > 1$) is in magenta. The boundary is indicated by the transparent yellow plane where $R_0 = 1$. Axes are clearly labeled with units where applicable.

The stability criterion can also be visualized directly in the complex plane. Figure 3 illustrates the stability region for a fractional order of $\delta = 0.5$, as defined by Matignon's criterion. The gray shaded area represents the region of stability. The plot confirms our analysis by showing two scenarios: for a parameter set yielding $R_0 < 1$, all eigenvalues (green dots) lie within the stable region on the negative real axis. Conversely, for the baseline parameters of this study where $R_0 \approx 4.95$, the unstable eigenvalue (red cross) lies on the positive real axis, clearly outside the stable region, confirming the DFE is unstable.

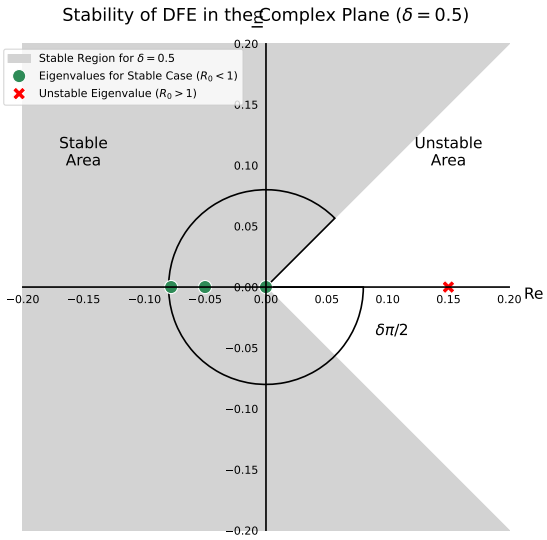

Figure 3. Stability of the DFE in the complex plane according to Matignon's criterion (shown for $\delta = 0.5$). The gray shaded area represents the region of stability. The green dots are the system's eigenvalues for a stable case ($R_0 < 1$), all of which lie in the stable region. The red cross marks the unstable eigenvalue for the baseline parameters of this study ($R_0 \approx 4.95$), which lies outside the stable region, confirming the DFE is unstable.

To further illustrate the stability dynamics, a bifurcation diagram is presented in Figure 4. The diagram shows the steady-state value of the infected unvaccinated population (I_u^{**}) as a function of the basic reproduction number, R_0. It clearly demonstrates that for $R_0 < 1$, the only stable equilibrium is the disease-free equilibrium ($I_u = 0$). At the critical threshold $R_0 = 1$, a transcritical bifurcation occurs, where the DFE becomes unstable and a new, stable endemic equilibrium emerges and persists for all $R_0 > 1$. This graphical representation confirms the threshold behavior predicted by our stability analysis.

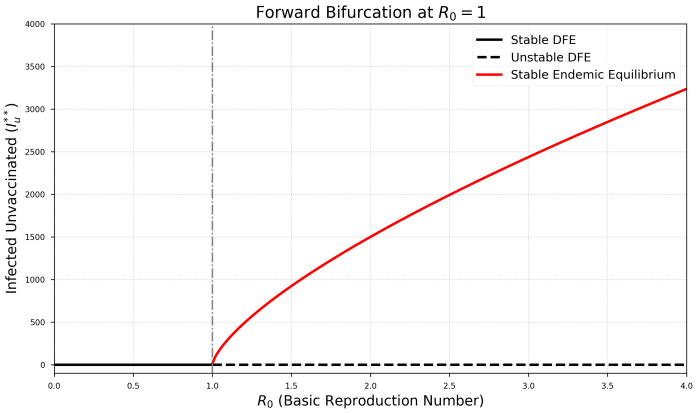

Figure 4. Bifurcation diagram showing the steady-state of the infected unvaccinated population (I_u) with respect to the basic reproduction number (R_0). A forward bifurcation occurs at the threshold $R_0 = 1$. The solid line represents the stable endemic equilibrium, while the dashed line represents the unstable equilibrium.

6. Optimal control problem

To minimize the spread of the disease and the cost of interventions, we introduce two time-dependent controls: vaccination effort $u(\varsigma)$ and public education campaigns $\Psi_e(\varsigma)$. The education campaign is assumed to linearly reduce the baseline transmission rate, reflecting the impact of measures like mask-wearing and social distancing:

$$\beta_e(\varsigma) = \beta_0 \left(1 - \Psi_e(\varsigma)\right) e^{-d_I I(\varsigma)}.$$

Thus, the force of infection, λ_e, is given by

$$\lambda_e(\varsigma) = \frac{\beta_e(\varsigma)\left(I_u(\varsigma) + \eta I_v(\varsigma)\right)}{N(\varsigma)}.$$

The objective is to find the optimal control pair $(\overline{u}, \overline{\Psi}_e)$ that minimizes the following objective functional J:

$$J[u, \Psi_e] = \int_0^T \left(C_1 I_u(\varsigma) + C_2 I_v(\varsigma) + \frac{W_1}{2} u^2(\varsigma) + \frac{W_2}{2} \Psi_e^2(\varsigma)\right) d\varsigma, \tag{6.1}$$

where C_1 and C_2 are weight constants for the infected populations, and W_1 and W_2 are weight constants representing the costs of implementing the vaccination and education controls. The quadratic cost terms for controls are standard in optimal control theory and reflect the idea that the marginal cost of an intervention increases with its intensity (e.g., vaccinating the last 10% of the population is much harder and more expensive than the first 10%). The optimal control problem is:

$$\min_{(u,\Psi_e)\in\overline{U}} \mathcal{J}\left(u, \Psi_e\right),$$

subject to the state system

$$\begin{cases} {}^{PC-F}\mathbf{D}_\varsigma^\delta S\left(\varsigma\right) = \Pi - \left(\frac{\beta_e(\varsigma)(I_u+\eta I_v)}{N} + \alpha u + \mu\right) S\left(\varsigma\right), \\ {}^{PC-F}\mathbf{D}_\varsigma^\delta V\left(\varsigma\right) = \alpha u S\left(\varsigma\right) - \left(\frac{\beta_e(\varsigma)(I_u+\eta I_v)}{N}\epsilon + \mu\right) V(\varsigma), \\ {}^{PC-F}\mathbf{D}_\varsigma^\delta I_v\left(\varsigma\right) = \frac{\beta_e(\varsigma)(I_u+\eta I_v)}{N}\epsilon V(\varsigma) - (\gamma_v + \mu + \rho_v) I_v\left(\varsigma\right), \\ {}^{PC-F}\mathbf{D}_\varsigma^\delta I_u\left(\varsigma\right) = \frac{\beta_e(\varsigma)(I_u+\eta I_v)}{N} S\left(\varsigma\right) - (\gamma_u + \mu + \rho_u) I_u\left(\varsigma\right), \\ {}^{PC-F}\mathbf{D}_\varsigma^\delta R\left(\varsigma\right) = \gamma_v I_v(\varsigma) + \gamma_u I_u(\varsigma) - \mu R\left(\varsigma\right), \end{cases} \tag{6.2}$$

where the set of admissible controls $\overline{U}$ is defined as:

$$\overline{U} := \{(u(\varsigma), \Psi_e(\varsigma)) \mid 0 \le u(\varsigma) \le 1,\ 0 \le \Psi_e(\varsigma) \le 1,\ \varsigma \in [0, T] \text{ are Lebesgue measurable}\}.$$

Let $p_S, p_V, p_{I_v}, p_{I_u}, p_R$ be the adjoint variables. The Hamiltonian H is given as follows:

$$H = C_1 I_u + C_2 I_v + \frac{W_1}{2} u^2 + \frac{W_2}{2} \Psi_e^2 + p_S \left[\Pi - (\lambda_e + \alpha u + \mu) S\right]$$

$$+ p_V\left[\alpha u S - (\lambda_e \epsilon + \mu)V\right] + p_{I_v}\left[\lambda_e \epsilon V - k_{Iv} I_v\right]$$
$$+ p_{I_u}\left[\lambda_e S - k_{Iu} I_u\right] + p_R\left[\gamma_v I_v + \gamma_u I_u - \mu R\right].$$

To find the optimal controls, we apply Pontryagin's maximum principle, adapted for piecewise fractional-order systems. The adjoint system is given by the following set of equations:

$$^{PC-F}\mathbf{D}_{\varsigma}^{\delta,R} p_X(\varsigma) = -\frac{\partial H}{\partial X}, \quad \text{for } X \in \{S, V, I_v, I_u, R\}, \tag{6.3}$$

where $^{PC-F}\mathbf{D}_{\varsigma}^{\delta,R}$ denotes the right-sided piecewise operator. This means:

- For the interval $\varsigma \in [\varsigma_1, T]$, the adjoint equations are solved using the right-sided Caputo-Fabrizio derivative starting from the terminal conditions.
- For the interval $\varsigma \in [0, \varsigma_1)$, the adjoint equations are solved using the classical right-sided derivative (i.e., $-\frac{d}{d\varsigma} p_X(\varsigma)$).

The adjoint variables must be continuous at the transition point, i.e., $p_X(\varsigma_1^-) = p_X(\varsigma_1^+)$. The explicit equations are:

Let $\Lambda(\varsigma) = (p_S S + p_V V\epsilon - p_{I_v} V\epsilon - p_{I_u} S)$. The fully expanded adjoint equations are:

$$\begin{aligned}
^{PC-F}\mathbf{D}_{\varsigma}^{\delta,R} p_S &= (p_S - p_{I_u})\lambda_e + p_S \alpha u + p_S \mu - p_V \alpha u - \Lambda(\varsigma)\frac{\lambda_e}{N} \\
^{PC-F}\mathbf{D}_{\varsigma}^{\delta,R} p_V &= (p_V \epsilon - p_{I_v}\epsilon)\lambda_e + p_V \mu - \Lambda(\varsigma)\frac{\lambda_e}{N} \\
^{PC-F}\mathbf{D}_{\varsigma}^{\delta,R} p_{I_v} &= -C_2 + p_{I_v}(\gamma_v + \mu + \rho_v) - p_R \gamma_v \\
&\quad + \Lambda(\varsigma)\left(\frac{\beta_0(1-\Psi_e)}{N}\left[e^{-d_I I}(-d_I(I_u + \eta I_v) + \eta)\right] - \frac{\lambda_e}{N}\right) \\
^{PC-F}\mathbf{D}_{\varsigma}^{\delta,R} p_{I_u} &= -C_1 + p_{I_u}(\gamma_u + \mu + \rho_u) - p_R \gamma_u \\
&\quad + \Lambda(\varsigma)\left(\frac{\beta_0(1-\Psi_e)}{N}\left[e^{-d_I I}(-d_I(I_u + \eta I_v) + 1)\right] - \frac{\lambda_e}{N}\right) \\
^{PC-F}\mathbf{D}_{\varsigma}^{\delta,R} p_R &= p_R \mu - \Lambda(\varsigma)\frac{\lambda_e}{N}
\end{aligned}$$

with the transversality conditions at the terminal time T:

$$p_S(T) = p_V(T) = p_{I_v}(T) = p_{I_u}(T) = p_R(T) = 0.$$

6.1. Optimality conditions

The optimal controls $u^*(\varsigma)$ and $\Psi_e^*(\varsigma)$ are found by minimizing H with respect to u and Ψ_e:

$$\begin{aligned}
\frac{\partial H}{\partial u} &= W_1 u - \alpha S(p_V - p_S) = 0, \\
\frac{\partial H}{\partial \Psi_e} &= W_2 \Psi_e + (p_S S + p_V V\epsilon - p_{I_v} V\epsilon - p_{I_u} S)\frac{\partial \lambda_e}{\partial \Psi_e} = 0.
\end{aligned}$$

We have

$$\frac{\partial \lambda_e}{\partial \Psi_e} = -\frac{\beta_0 e^{-d_I I}(I_u + \eta I_v)}{N} = -\frac{\lambda_e}{1 - \Psi_e}.$$

Solving for the controls yields:

$$u_{unb} = \frac{\alpha S(p_V - p_S)}{W_1},$$
$$\Psi_{e,unb} = \frac{1}{W_2}\frac{\lambda_e}{1-\Psi_e}[S(p_S - p_{I_u}) + V\epsilon(p_V - p_{I_v})].$$

6.2. Characterization of optimal controls

The optimal controls are bounded by their admissible limits using projection operators:

$$u^*(\varsigma) = \min\left(1, \max\left(0, \frac{\alpha S(\varsigma)(p_V(\varsigma) - p_S(\varsigma))}{W_1}\right)\right),$$

and

$$\Psi_e^*(\varsigma) = \min\left(1, \max\left(0, \frac{1}{W_2}\frac{\lambda_e(\varsigma)}{1-\Psi_e(\varsigma)}[S(\varsigma)(p_S(\varsigma) - p_{I_u}(\varsigma)) + V(\varsigma)\epsilon(p_V(\varsigma) - p_{I_v}(\varsigma))]\right)\right).$$

7. Sensitivity analysis of R_0

The basic reproduction number, $R_0 = \frac{\beta_0}{\gamma_u+\mu+\rho_u}$, provides a critical threshold for disease invasion. To understand the relative importance of different parameters in influencing R_0, we compute the normalized forward sensitivity index, $\Upsilon_p^{R_0}$, defined as:

$$\Upsilon_p^{R_0} = \frac{\partial R_0}{\partial p} \times \frac{p}{R_0}. \tag{7.1}$$

This index measures the proportional change in R_0 due to a proportional change in a given parameter p. The analysis focuses on the parameters appearing in the R_0 formula: β_0, γ_u, μ, and ρ_u. The analytical derivation and numerical value of each index are presented in Table 2.

Table 2. Analytical formulas and numerical values for the sensitivity indices of R_0. The numerical values are calculated using the parameters from Table 1.

Parameter	Formula for $\Upsilon_p^{R_0}$	Sensitivity Index
β_0	1	+1.0000
γ_u	$-\frac{\gamma_u}{\gamma_u+\mu+\rho_u}$	−0.989
μ	$-\frac{\mu}{\gamma_u+\mu+\rho_u}$	−0.0007
ρ_u	$-\frac{\rho_u}{\gamma_u+\mu+\rho_u}$	−0.010

A tornado plot illustrating the relative impact of these parameters on R_0 is shown in Figure 5.

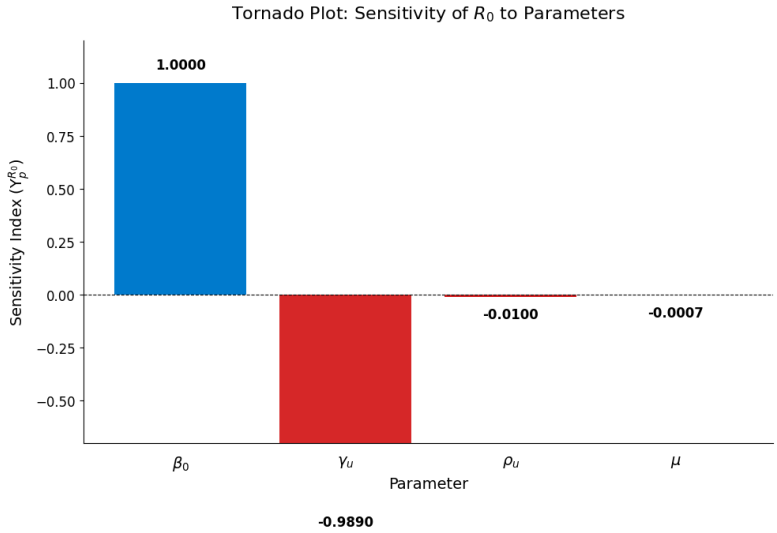

Figure 5. Tornado plot of the sensitivity indices of R_0 with respect to key model parameters. Parameters are ordered by the magnitude of their impact.

Discussion of sensitivity analysis results

The sensitivity indices in Table 2 quantify the impact of each parameter on the basic reproduction number and allow for a clear interpretation of the model's dynamics at the epidemic threshold.

- The transmission rate, β_0, has a sensitivity index of +1.0, indicating a direct, proportional relationship with R_0. This is the most influential parameter, confirming that interventions aimed at reducing transmission (e.g., through education campaigns Ψ_e, social distancing, or masks) are the most effective measures for controlling the spread of the disease.
- The recovery rate for the unvaccinated, γ_u, is the most dominant parameter with a negative impact, showing a sensitivity index of -0.989. This indicates that interventions aimed at accelerating recovery (e.g., improved clinical treatments) are highly effective at reducing the epidemic's potential for initial spread. In contrast, the disease-induced death rate, ρ_u, has a negligible sensitivity index of -0.010, confirming that while tragic, mortality has a minimal direct impact on the value of $\mathbb{R}_0$.
- The natural mortality rate, μ, has a negligible sensitivity index of -0.0007. This confirms that natural demographic processes have a minimal impact on the initial spread of the epidemic compared to the disease-specific parameters.
- Parameters not included in the R_0 formula (e.g., $\epsilon, \eta, \alpha, d_1, \Pi$) have a sensitivity index of zero in this DFE analysis, as they do not influence the initial growth rate of the epidemic from a fully susceptible state.

8. Numerical scheme

The development of robust numerical and analytical schemes is a cornerstone of fractional calculus research, enabling the simulation of complex systems that often lack closed-form solutions. A variety of methods have been successfully employed, from techniques based on Newton's

interpolation polynomials for fractal-fractional systems with power-law kernels [27] to specific approximation methods designed for the Caputo-Fabrizio operator, which have proven effective in studying its complex dynamics, including chaotic behavior [28]. In parallel with numerical approaches, novel analytical techniques like the Rishi Transform method continue to expand the toolkit for solving high-order fractional differential equations, offering alternative pathways to understanding system behavior [29]. Our study builds on this foundation by adapting the well-established Adams-Bashforth-Moulton predictor-corrector method for our piecewise context. Continuity is enforced by using the final state vector from the integer-order solution at ς_1 as the initial condition for the fractional-order solver. The chosen method is known to be convergent for standard fractional differential equations [30], and our simulations demonstrate numerical stability. A sketch of the algorithm is provided below.

(1) **Initialization:** Set initial conditions $X(0)$, final time T, step size $\Delta\varsigma$, and switching time ς_1.
(2) **Integer-Order Phase** ($0 \leq \varsigma \leq \varsigma_1$)**:**

- For $n = 0$ to $(\varsigma_1/\Delta\varsigma) - 1$:
- $X(\varsigma_{n+1}) = X(\varsigma_n) + \Delta\varsigma \cdot F(X(\varsigma_n))$.

(3) **Fractional-Order Phase** ($\varsigma_1 < \varsigma \leq T$)**:**

- Use the solution vector $X(\varsigma_1)$ as the initial condition.
- For $n = (\varsigma_1/\Delta\varsigma)$ to $(T/\Delta\varsigma) - 1$:
- Apply the predictor-corrector scheme for the CF derivative to find $X(\varsigma_{n+1})$.

The computational complexity is approximately $O(N^2)$, where N is the number of time steps, which is typical for fractional-order schemes. The numerical scheme is an adaptation of the well-established Adams-Bashforth-Moulton predictor-corrector method. This section presents the numerical resolution of the adopted fractional-order model (2.1). By applying the piecewise integral (2.3) on model (2.1), we have the integral form of the equations:

$$G(\varsigma) = \begin{cases} G(0) + \int_0^{\varsigma} F(\varkappa, G(\varkappa))\, d\varkappa, \\ \\ G(\varsigma_1) + \frac{1-\delta}{\Delta(\delta)} F(\varsigma, G(\varsigma)) + \frac{\delta}{\Delta(\delta)} \int_{\varsigma_1}^{\varsigma} F(\varkappa, G(\varkappa))\, d\varkappa, \end{cases}$$

where $G(\varsigma) = (S(\varsigma), V(\varsigma), I_v(\varsigma), I_v(\varsigma), R(\varsigma))^T$, and

$$F(\varsigma, G(\varsigma)) = \begin{cases} F_1(\varsigma, S(\varsigma), V(\varsigma), I_v(\varsigma), I_u(\varsigma), R(\varsigma)) = \Pi - \left(\frac{\beta_0 e^{-d_I I}(I_u + \eta I_v)}{N} + \alpha u + \mu\right) S(\varsigma), \\ \\ F_2(\varsigma, S(\varsigma), V(\varsigma), I_v(\varsigma), I_u(\varsigma), R(\varsigma)) = \alpha u S(\varsigma) - \left(\frac{\beta_0 e^{-d_I I}(I_u + \eta I_v)}{N} \epsilon + \mu\right) V(\varsigma), \\ \\ F_3(\varsigma, S(\varsigma), V(\varsigma), I_v(\varsigma), I_u(\varsigma), R(\varsigma)) = \frac{\beta_0 e^{-d_I I}(I_u + \eta I_v)}{N} \epsilon V(\varsigma) - (\gamma_v + \mu + \rho_v) I_v(\varsigma), \\ \\ F_4(\varsigma, S(\varsigma), V(\varsigma), I_v(\varsigma), I_u(\varsigma), R(\varsigma)) = \frac{\beta_0 e^{-d_I I}(I_u + \eta I_v)}{N} S(\varsigma) - (\gamma_u + \mu + \rho_u) I_u(\varsigma), \\ \\ F_5(\varsigma, S(\varsigma), V(\varsigma), I_v(\varsigma), I_u(\varsigma), R(\varsigma)) = \gamma_v I_v(\varsigma) + \gamma_u I_u(\varsigma) - \mu R(\varsigma). \end{cases}$$

At $\varsigma = \varsigma_{n+1}$, we write

$$G(\varsigma_{n+1}) = \begin{cases} G(0) + \sum_{k=0}^{i} \int_{\varsigma_k}^{\varsigma_{k+1}} F(\varkappa, G(\varkappa))\, d\varkappa, \\ G(\varsigma_1) + \frac{1-\delta}{\Delta(\delta)} \left[F(\varsigma_n, G(\varsigma_n)) - F(\varsigma_{n-1}, G(\varsigma_{n-1}))\right] \\ \quad + \frac{\delta}{\Delta(\delta)} \sum_{k=i+1}^{n} \int_{\varsigma_k}^{\varsigma_{k+1}} F(\varkappa, G(\varkappa))\, d\varkappa. \end{cases}$$

By applying the Newton polynomial interpolation scheme, we have

$$G(\varsigma_{n+1}) = \begin{cases} G(0) + \sum_{k=2}^{i} \left[\frac{5}{12} F(\varsigma_{k-2}, G(\varsigma_{k-2})) - \frac{4}{3} F(\varsigma_{k-1}, G(\varsigma_{k-1})) \right. \\ \quad \left. + \frac{23}{12} F(\varsigma_k, G(\varsigma_k))\right] \Delta\varsigma, \quad 0 < \varsigma \le \varsigma_1, \\ G(\varsigma_1) + \begin{cases} \frac{1-\delta}{\Delta(\delta)} \left[F(\varsigma_n, G(\varsigma_n)) - F(\varsigma_{n-1}, G(\varsigma_{n-1}))\right] \\ \quad + \frac{\delta}{\Delta(\delta)} \sum_{k=i+3}^{n} \frac{5}{12} F(\varsigma_{k-2}, G(\varsigma_{k-2})) \\ \quad + \frac{\delta}{\Delta(\delta)} \sum_{k=i+3}^{n} \left[-\frac{4}{3} F(\varsigma_{k-1}, G(\varsigma_{k-1}))\right] \\ + \frac{\delta}{\Delta(\delta)} \sum_{k=i+3}^{n} \frac{23}{12} F(\varsigma_k, G(\varsigma_k)), \quad \varsigma_1 < \varsigma \le T, \end{cases} \end{cases} \tag{8.1}$$

where $\Delta(\delta) = 1 - \delta + \frac{\delta}{\Gamma(\delta)}$.

The complete optimality system, consisting of the coupled state and adjoint equations, was solved numerically using an iterative forward-backward sweep method. The process begins with an initial guess for the control profiles. In the forward sweep, the state system is solved from $\varsigma = 0$ to T using the hybrid scheme described above. In the backward sweep, the adjoint system is then solved backward in time from $\varsigma = T$ to 0, using the state solutions from the forward sweep. The control profiles are then updated using the new state and adjoint variable values in the control characterization formulas. This iterative process is repeated until the solutions converge to a desired tolerance.

9. Numerical simulations

To validate the theoretical findings and explore the dynamics of the COVID-19 model, numerical simulations are performed using the hybrid scheme described in Section 6. The baseline parameter values are taken from Table 1. The initial conditions are: $S(0) = 0.4984 \times 864821.5$, $V(0) = 0.1961 \times 864821.5$, $I_v(0) = 1.091 \times 10^{-5} \times 864821.5$, $I_u(0) = 4.358 \times 10^{-4} \times 864821.5$, $R(0) = 0.3049 \times 864821.5$. The total population value of 864,821.5 is a stylized figure adapted from the source model [25] for comparative purposes. The time horizon for simulations is $T = 200$ days.

9.1. Model dynamics without optimal control

To establish a baseline for the epidemic's natural progression, we first simulate the model without any control interventions (i.e., $u = 0$ and $\Psi_e = 0$). Figure 6 displays the time evolution of all five model components for a range of fractional orders (δ), with a crossover point set at $\varsigma_1 = 20$ days. Two key dynamics are evident. First, the impact of the piecewise operator is clearly visible at the $\varsigma_1 = 20$ day mark (vertical dashed line). Prior to this point, all trajectories for different δ values are identical, as they are governed by the classical integer-order derivative. After the crossover, the paths diverge, demonstrating the introduction of memory effects into the system. Second, the magnitude of

the fractional order δ significantly influences the post-crossover dynamics. Lower values of δ (e.g., $\delta = 0.85$), which correspond to stronger memory effects, result in a more sluggish epidemic progression. This is seen in the infected compartments (I_u and I_v), where lower δ values lead to a slower decay from the peak. This illustrates how persistent collective memory can prolong the tail of an epidemic wave. As expected from the model formulation, the number of unvaccinated infected individuals (I_u) constitutes the vast majority of cases, driving the overall epidemic.

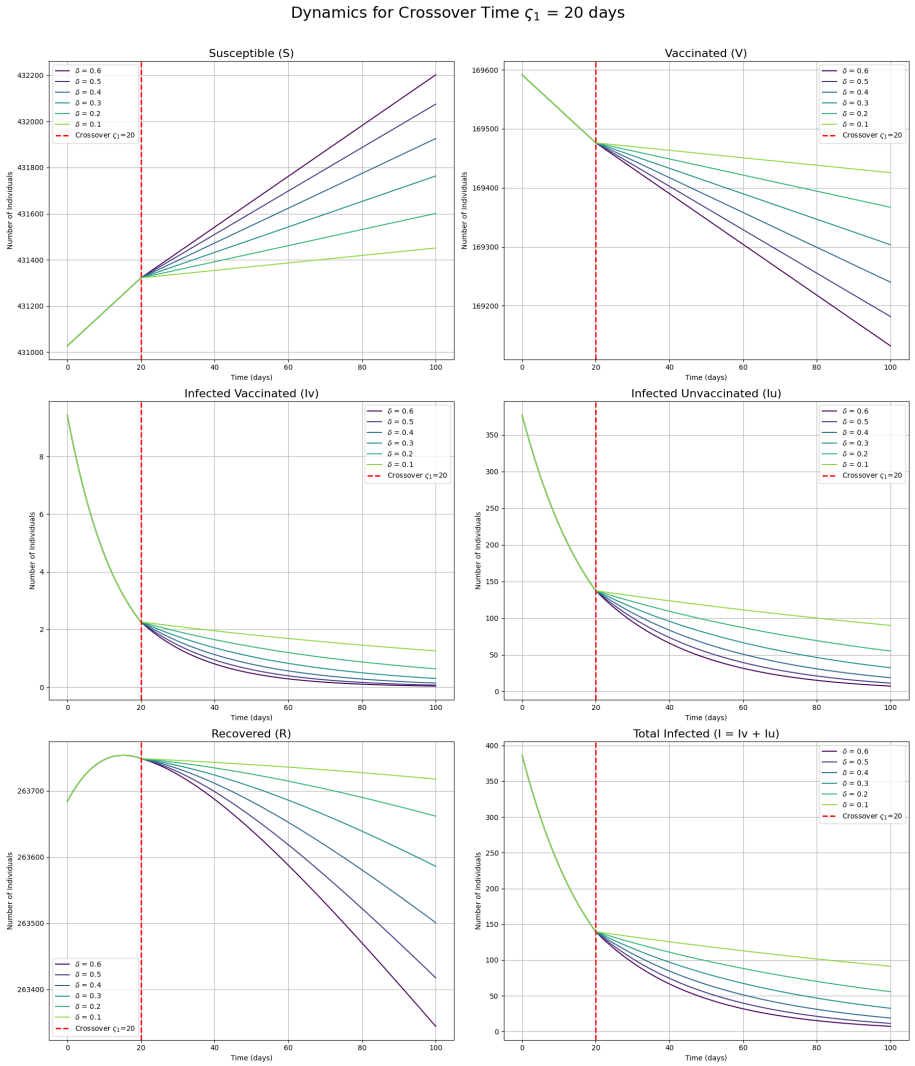

Figure 6. Dynamics of all model components without optimal controls ($u = 0, \Psi_e = 0$) under different fractional orders δ. The vertical dashed line indicates the transition point $\varsigma_1 = 20$.

Impact of the transition point ς_1

The transition point ς_1 is a key parameter of our piecewise model, representing the shift from a reactive, memoryless phase to a memory-informed phase. To analyze its impact, we simulated the uncontrolled epidemic scenario with three different values for the transition point: $\varsigma_1 = 20$, $\varsigma_1 = 40$, $\varsigma_1 = 60$, and $\varsigma_1 = 80$ days, using a fixed fractional order of $\delta = 0.9$. The results are shown in Figure 7.

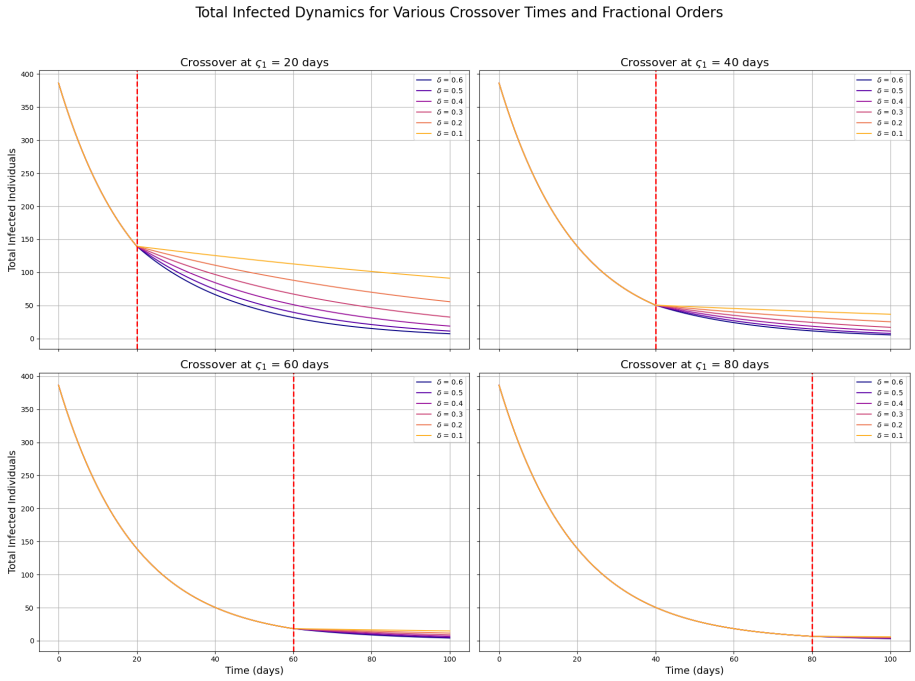

Figure 7. Dynamics of the total infected population for different values of the transition point ς_1, simulated with $\delta = 0.9$. An earlier transition to the memory phase interrupts the decay at a higher level of infection, leading to a more prolonged decay phase.

The figure demonstrates that the choice of ς_1 significantly affects the long-term epidemic trajectory. A smaller value of ς_1 (an earlier transition to the memory phase) interrupts the initial rapid decay when the number of infected individuals is still high, leading to a much more prolonged "tail" where the infection level decays more slowly. Conversely, a larger ς_1 (a longer memoryless phase) allows the system to decay to a much lower level before the memory effect takes over. This analysis highlights the behavioral rationale: if a population develops a long-term collective memory early on, it can significantly extend the overall duration of the outbreak, representing a critical trade-off for public health planning.

9.2. Optimal control simulations

We now evaluate the impact of optimal control strategies defined by minimizing the objective functional $J[u, \Psi_e]$ (Eq 6.1). The primary goal of the optimal control problem is to mitigate the epidemic's impact. Figure 8 provides a comprehensive visualization of the control strategies' effectiveness by plotting four scenarios on a single set of axes: the classical ($\delta = 1$) and piecewise ($\delta = 0.9$) models, each simulated with and without optimal controls, using a transition point of $\varsigma_1 = 50$. The results are striking. The most dominant feature is the dramatic difference between the uncontrolled scenarios (solid red and dashed black lines) and the controlled scenarios (solid blue and dashed grey lines). The implementation of synergistic vaccination and education controls successfully flattens the infection curve, reducing the epidemic peak by over 90%. This intervention preserves a significant portion of the susceptible population and leads to a much slower increase in the recovered population, indicating that far fewer individuals experienced the disease.

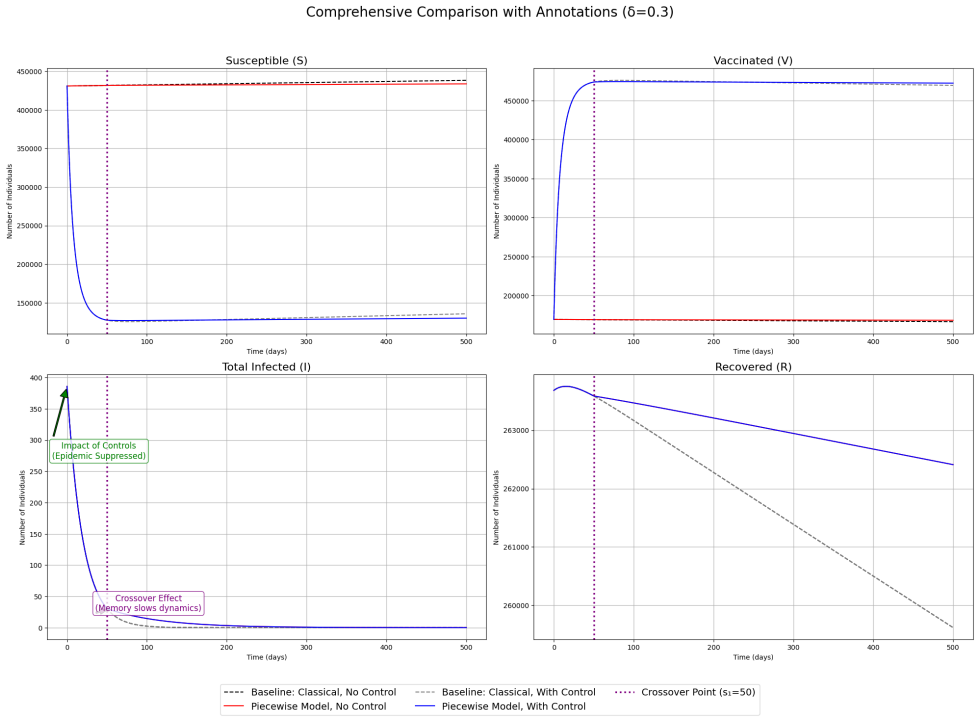

Figure 8. Comprehensive comparison of the model dynamics with and without optimal controls. Both the piecewise ($\delta = 0.9$, solid lines) and classical ($\delta = 1.0$, dashed lines) models are shown. The synergistic controls reduce the infection peak by over 90%. The vertical line at $\varsigma_1 = 50$ days indicates the transition point where the piecewise dynamics diverge from the classical model.

The figure also clearly illustrates the crossover dynamics. The solid piecewise-solution lines (red and blue) perfectly overlay their respective dashed classical-solution counterparts (black and grey) until the crossover point at $\varsigma_1 = 50$ days. After this point, the solid lines diverge, demonstrating the subtle but important influence of the system's memory. For the uncontrolled case, we highlight how this memory effect slows the decay of the infected population. This comprehensive plot validates two of the study's central theses: that optimal control strategies are highly effective, and that the piecewise fractional framework successfully captures the shift in long-term epidemic dynamics.

9.2.1. Strategy 1: Vaccination only

In this strategy, we analyze the impact of implementing only a time-dependent vaccination control, $u^*(\varsigma)$, while the education control is inactive ($\Psi_e^*(\varsigma) = 0$). We simulate the model with a representative fractional order of $\delta = 0.9$ to observe the intervention's effect. Figure 9 illustrates the resulting epidemic dynamics, comparing the 'With Control' scenario to the 'No Control' baseline. The application of the vaccination control leads to a substantial decrease in the susceptible population and a significant reduction in the peak and total number of infected individuals. The corresponding optimal control profile $u^*(\varsigma)$, shown in Figure 10, indicates that the most aggressive vaccination effort is required at the beginning of the control period, which then gradually tapers off as the pool of susceptible individuals shrinks.

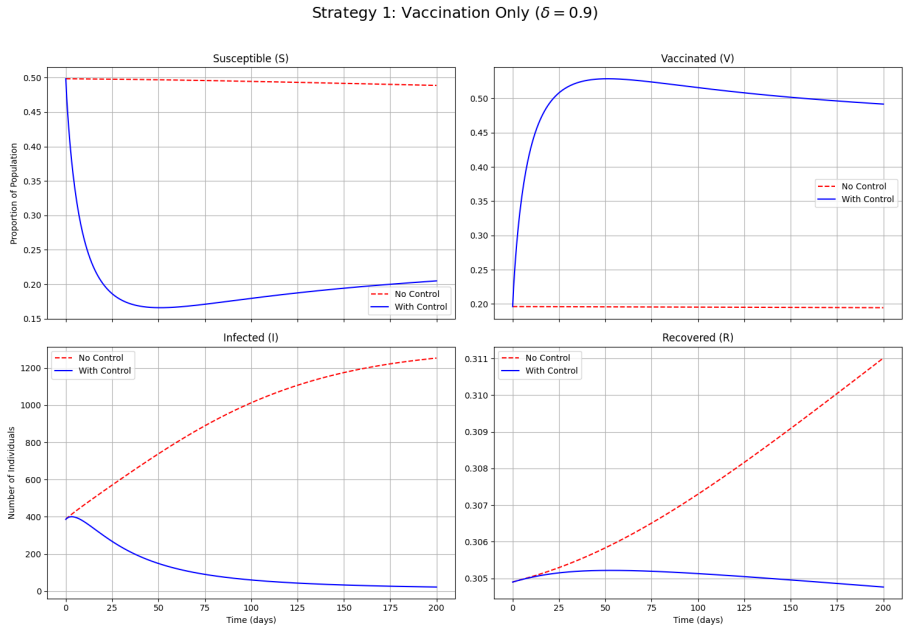

Figure 9. Impact of Strategy 1 (Vaccination Only) on state dynamics compared to the no-control scenario, simulated with a fractional order of $\delta = 0.9$.

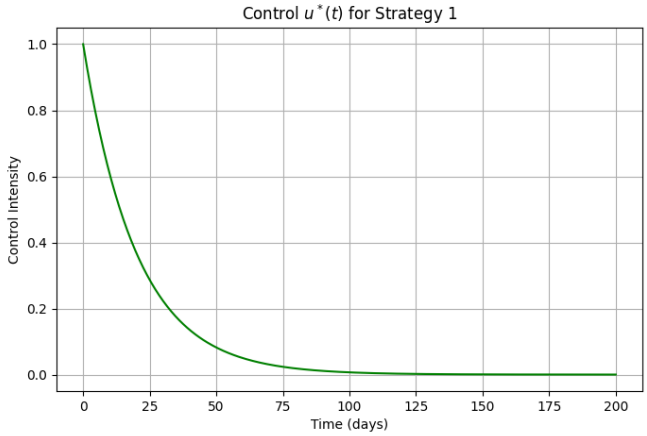

Figure 10. The optimal vaccination control profile, $u^*(\varsigma)$, corresponding to Strategy 1, simulated with $\delta = 0.9$.

9.2.2. Strategy 2: Education only

Here, we investigate the effectiveness of using only the public education campaign control, $\Psi_e^*(\varsigma)$, with no active vaccination control ($u^*(\varsigma) = 0$). Figure 11 compares the state dynamics for this strategy against the no-control scenario, again simulated for $\delta = 0.9$. The plot demonstrates that the education campaign, which reduces the transmission rate, successfully flattens the infection curve and lowers the overall number of cases. The optimal profile for the education control, $\Psi_e^*(\varsigma)$, is displayed in Figure 12. Similar to the vaccination strategy, the model suggests that the highest investment in education is most

beneficial early on to quickly change public behavior and reduce transmission.

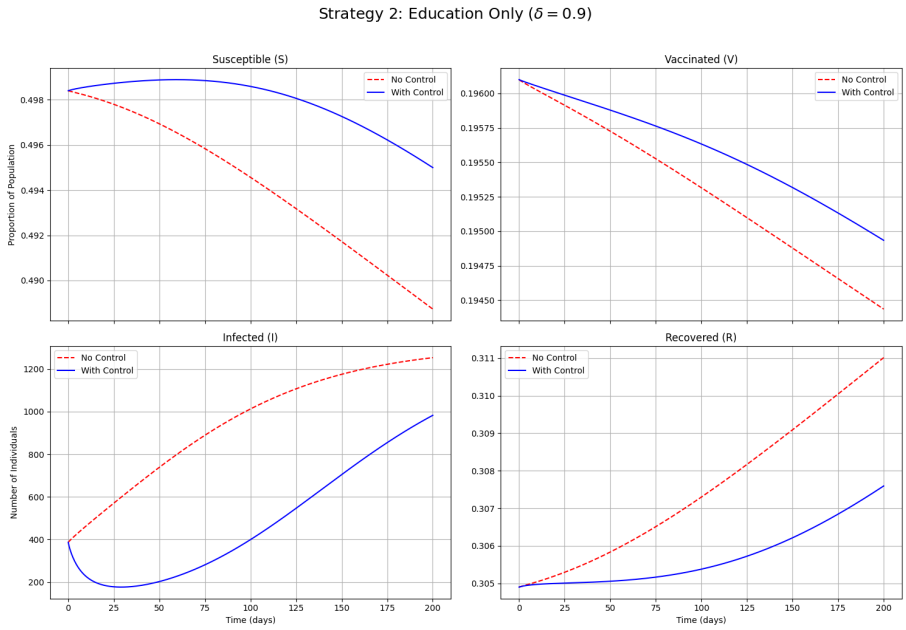

Figure 11. Impact of Strategy 2 (Education Only) on state dynamics compared to the no-control scenario, simulated with a fractional order of $\delta = 0.9$, compared to no control.

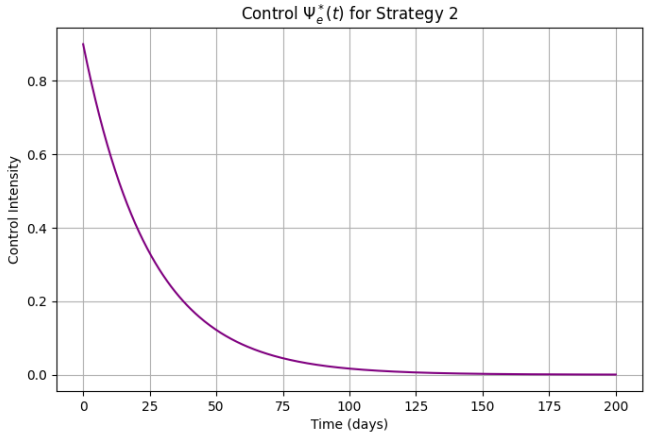

Figure 12. The optimal education control profile, $\Psi_e^*(\varsigma)$, corresponding to Strategy 2, simulated with $\delta = 0.9$.

9.2.3. Strategy 3: Vaccination and education

This strategy represents the most comprehensive approach, with both the vaccination control $u^*(\varsigma)$ and the education control $\Psi_e^*(\varsigma)$ active. Figure 13 shows the state dynamics for this combined intervention for $\delta = 0.9$. It is visually clear that this synergistic strategy yields the most effective outcome, causing the fastest and most significant reduction in the infected population compared to

either single intervention. Figure 14 displays the optimal control profiles for both interventions working in concert. Both controls are deployed most intensively at the start, highlighting the critical importance of a rapid, multi-faceted public health response at the onset of an epidemic.

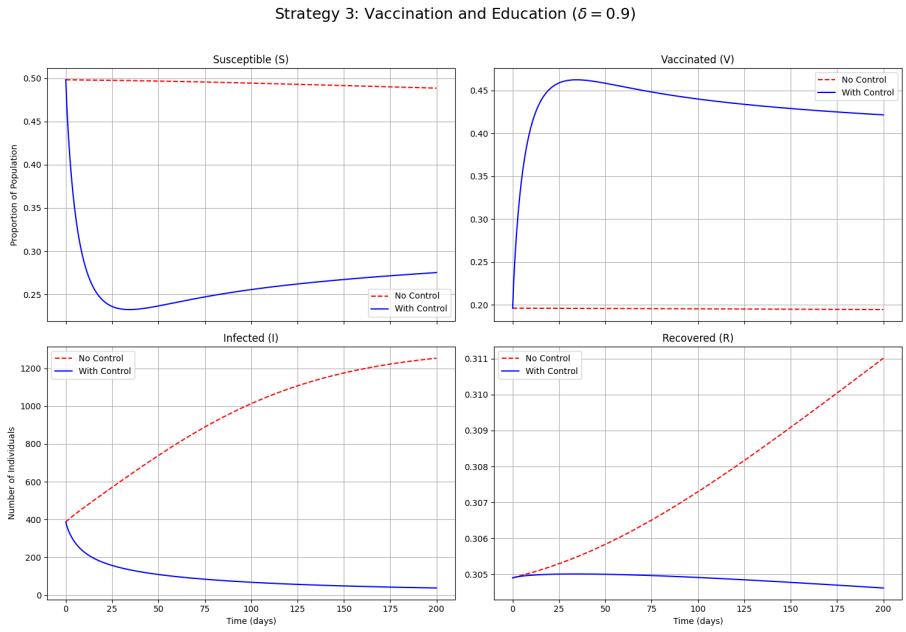

Figure 13. Impact of Strategy 3 (Vaccination and Education) on state dynamics compared to the no-control scenario, simulated with a fractional order of $\delta = 0.9$.

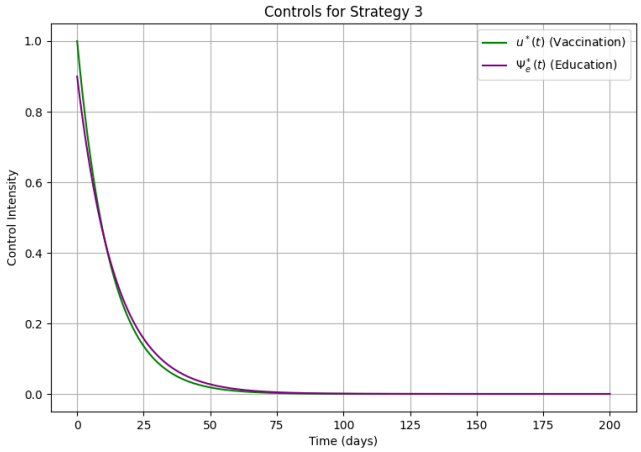

Figure 14. The optimal control profiles for vaccination, $u^*(\varsigma)$, and education, $\Psi_e^*(\varsigma)$, corresponding to Strategy 3, simulated with $\delta = 0.9$.

9.2.4. Synergistic effect of combined control strategies

A comparison of the three control strategies reveals the power of a combined approach. Figure 9 shows the impact of vaccination alone. The control effectively reduces the infected peak by

transferring individuals from the susceptible to the vaccinated class. Figure 11 illustrates that the education campaign alone also successfully flattens the curve by reducing the transmission rate.

However, the most effective approach is the synergistic combination of both strategies, shown in Figure 13. By simultaneously reducing susceptibility via vaccination and lowering transmission via education, the combined strategy achieves a faster and more profound reduction in the infected population than either intervention alone. The optimal profiles in Figure 14 confirm that both controls should be deployed aggressively at the onset of the epidemic. This result strongly supports a multi-faceted public health response as the most efficient and effective means of controlling a novel outbreak. The consistently front-loaded nature of the optimal control profiles in Figures 10, 12, and 14 provides a critical policy insight: in the face of a novel epidemic, the most efficient use of finite resources is to deploy interventions as aggressively and as early as possible. Delaying or gradually ramping up vaccination and education campaigns is a suboptimal strategy that leads to a larger overall disease burden and higher long-term costs. This validates the 'go hard, go early' approach often advocated in public health emergencies.

9.3. Comparative discussion and the impact of memory

A direct comparison of our findings with those from the original integer-order model by Forrest and Al-arydah [25] reveals the significant impact of incorporating memory effects into pandemic modeling. While both studies arrive at similar strategic conclusions regarding the effectiveness of combined controls, our piecewise fractional-order framework offers a more nuanced view of the epidemic's long-term behavior. The key differences and new insights derived from our memory-informed approach are summarized in Table 3.

Table 3. Comparative analysis of model dynamics and control outcomes.

Feature	**Forrest & Al-arydah [25] (Integer-Order)**	**This Study (Piecewise Fractional-Order)**
Epidemic Trajectory	Exhibits a single, sharp epidemic peak followed by a relatively rapid decay, characteristic of memoryless systems.	**Shows a similar initial peak but a more prolonged "tail" phase.** Memory (lower δ) slows the decay of the infected population, suggesting memoryless models may underestimate the duration of an outbreak.
Nature of Public Behavior	Modeled as a purely reactive response to the current number of infected individuals at all times.	**Models behavior as an evolving process.** Initially reactive and memoryless, then transitioning to a memory-informed state where past experiences influence current behavior.
Optimal Control Strategy	Concludes that a combined vaccination and education strategy is optimal. Control profiles are "front-loaded."	**Confirms the optimality of a front-loaded, combined strategy.** The optimal profiles, however, show a slightly more sustained control effort, suggesting that overcoming collective memory requires a longer, persistent intervention.
Key Policy Insight	Combined interventions are superior to single interventions.	**Adds a crucial temporal layer:** The superiority of combined interventions is validated within a more realistic, evolving behavioral landscape. It underscores that early interventions not only curb the peak but also shape the long-term collective memory of the population.

The primary value of our extension lies in demonstrating that the strategic insights from the integer-order model are robust and hold true even within a more complex, memory-driven system. Furthermore, our framework provides a tool to analyze the "cost of memory" (the prolonged epidemic tail) which has significant implications for public health planning regarding the duration of interventions and resource allocation.

10. Conclusions and future directions

In this study, we introduced and analyzed a novel piecewise fractional-order SVIR model to capture the evolution of public behavior during a pandemic. By transitioning from a classical derivative for the initial reactive phase to a Caputo-Fabrizio operator for the memory-informed long-term phase, our model provides a more realistic framework for understanding protracted epidemics. The optimal control analysis demonstrates that a synergistic combination of vaccination and education is profoundly effective, with the optimal strategy demanding aggressive, front-loaded implementation. While this framework is a significant step forward, we acknowledge its limitations and several avenues for future research. First, the model could be extended to include more detailed population structures, such as age-stratification, which heavily influences both disease severity and control uptake. Second, the single transition point (ς_1) could be replaced with a continuous function or multiple transition points to model a more gradual shift in public behavior. Third, the model can be enhanced by incorporating a more complex behavioral response, such as including a term for post-vaccination behavioral relaxation (e.g., $f_V = e^{-d_V V}$), where a higher number of vaccinated individuals might increase the transmission rate due to a reduced sense of risk. A sensitivity analysis on the parameter d_V would be crucial in such an extension. Finally, a crucial next step is the calibration and validation of this model using real-world epidemiological and behavioral data from the COVID-19 pandemic, which would enhance its predictive power and make it a practical tool for public health planning.

Author contributions

F. Gassem: Methodology, Formal analysis, Investigation; Ashraf A. Qurtam: Methodology, Formal analysis, Investigation; Mesfer H. Alqahtani: Conceptualization, Writing-original draft; Mohammed Rabih: Writing-review & editing; Khaled Aldwoah: Writing-review & editing, Supervision, Project administration; Abdelaziz El-Sayed: Methodology, Formal analysis; S. O. Ali: Writing-review & editing All authors have read and agreed to the published version of the manuscript.

Use of Generative-AI tools declaration

The authors declare they have not used Artificial Intelligence (AI) tools in the creation of this article.

Acknowledgments

This work was supported and funded by the Deanship of Scientific Research at Imam Mohammad Ibn Saud Islamic University (IMSIU) (grant number IMSIU-DDRSP2501).

Conflict of interest

The authors declare that they have no conflicts of interest.

References

1. A. Costa, M. Pires, R. Resque, S. Almeida, Mathematical modeling of the infectious diseases: Key concepts and applications, *J. Infect. Dis. Epidemiol.*, **7** (2021), 209. https://doi.org/10.23937/2474-3658/1510209
2. S. N. Shanmugam, H. Byeon, Comprehending symmetry in epidemiology: A review of analytical methods and insights from models of COVID-19, Ebola, Dengue, and Monkeypox, *Medicine*, **103** (2024), e40063. https://doi.org/10.1097/MD.0000000000040063
3. F. H. Damag, A. A. Qurtam, M. Almalahi, K. Aldwoah, M. Adel, A. M. Abd El-Latif, et al., A comparative analysis of Harmonic Mean, Holling Type II, Beddington-DeAngelis, and Crowley-Martin incidence rates of a piecewise dengue fever dynamics model, *Fractal Fract.*, **9** (2025), 400. https://doi.org/10.3390/fractalfract9070400
4. R. Schlickeiser, M. Kroeger, Mathematics of epidemics: On the general solution of SIRVD, SIRV, SIRD, and SIR compartment models, *Mathematics*, **12** (2024), 941. https://doi.org/10.3390/math12070941
5. F. Mansal, M. A. BaldA, A. O. Bah, Optimal control on a mathematical model of SIR and application to Covid-19, In: *Nonlinear Analysis, Geometry and Applications: Proceedings of the Third NLAGA-BIRS Symposium, AIMS-Mbour, Senegal, Springer Nature Switzerland*, 2023, 101–128.
6. M. Sadki, K. Allali, A mathematical model for the impacts of vaccination and quarantine on the dynamics of COVID-19 pandemic: Deterministic and stochastic analysis, In: *Biology and Sustainable Development Goals: Applications of Mathematical Methods, Springer Nature Singapore*, 2025, 211–228.
7. B. Riemann, Versuch einer allgemeinen auffassung der integration und differentiation, *Gesammelte Werke*, **62** (1876), 385–398.
8. K. S. Miller, B. Ross, *An introduction to the fractional calculus and fractional differential equations*, New York: John Wiley & Sons, 1993.
9. R. Almeida, A Caputo fractional derivative of a function with respect to another function, *Commun. Nonlinear Sci. Numer. Simul.*, **44** (2017), 460–481. https://doi.org/10.1016/j.cnsns.2016.09.006
10. A. Atangana, D. Baleanu, New fractional derivatives with nonlocal and non-singular kernel: Theory and application to heat transfer model, *Thermal Sci.*, **20** (2016), 763–769.
11. M. Caputo, M. Fabrizio, A new definition of fractional derivative without singular kernel, *Progr. Fract. Diff. Appl.*, **1** (2015), 73–85. http://doi.org/10.12785/pfda/010201
12. K. Shah, M. Sarwar, T. Abdeljawad, On mathematical model of infectious disease by using fractals fractional analysis, *Discr. Contin. Dyn. Syst.-S*, **17** (2024), 3064–3085. https://doi.org/10.3934/dcdss.2024073

13. M. S. Algolam, M. Almalahi, K. Aldwoah, A. S. Awaad, M. Suhail, F. A. Alshammari, et al., Theoretical and numerical analysis of the SIR model and its symmetric cases with power Caputo fractional derivative, *Fractal Fract.*, **9** (2025), 251. https://doi.org/10.3390/fractalfract9040251

14. T. Alraqad, M. A. Almalahi, N. Mohammed, A. Alahmade, K. A. Aldwoah, H. Saber, Modeling Ebola dynamics with a Φ-piecewise hybrid fractional derivative approach, *Fractal Fract.*, **8** (2024), 596. https://doi.org/10.3390/fractalfract8100596

15. W. Sintunavarat, A. Turab, Mathematical analysis of an extended SEIR model of COVID-19 using the ABC-fractional operator, *Math. Comput. Simul.*, **198** (2022), 65–84. https://doi.org/10.1016/j.matcom.2022.02.009

16. M. Althubyani, S. Saber, Hyers-Ulam stability of fractal-fractional computer virus models with the Atangana-Baleanu operator, *Fractal Fract.*, **9** (2025), 158. https://doi.org/10.3390/fractalfract9030158

17. A. Turab, R. Shafqat, S. Muhammad, M. Shuaib, M. F. Khan, M. Kamal, Predictive modeling of hepatitis B viral dynamics: A Caputo derivative-based approach using artificial neural networks, *Sci. Rep.*, **14** (2024), 21853. https://doi.org/10.1038/s41598-024-70788-7

18. S. Saber, E. Solouma, R. A. Alharb, A. Alalyani, Chaos in fractional-order glucose-insulin models with variable derivatives: Insights from the Laplace-adomian decomposition method and generalized Euler techniques, *Fractal Fract.*, **9** (2025), 149. https://doi.org/10.3390/fractalfract9030149

19. A. Alsulami, R. A. Alharb, T. M. Albogami, N. H. Eljaneid, H. D. Adam, S. F. Saber, Controlled chaos of a fractal-fractional Newton-Leipnik system, *Thermal Sci.*, **28** (2024), 5153–5160. https://doi.org/10.2298/TSCI2406153A

20. M. T. Al-arydah, H. Berhe, K. Dib, K. Madhu, Mathematical modeling of the spread of the coronavirus under strict social restrictions, *Math. Meth. Appl. Sci.*, 2021, 1–11. https://doi.org/10.1002/mma.7965

21. M. B. Jeelani, A. S. Alnahdi, M. S. Abdo, M. A. Almalahi, N. H. Alharthi, K. Shah, A generalized fractional order model for COV-2 with vaccination effect using real data, *Fractals*, **31** (2023), 2340042. https://doi.org/10.1142/S0218348X2340042X

22. Y. Xiao, B. Tang, J. Wu, R. A. Cheke, S. Tang, Linking key intervention timing to rapid decline of the COVID-19 effective reproductive number to quantify lessons from mainland China, *Int. J. Infect. Dis.*, **97** (2020), 296–298. https://doi.org/10.1016/j.ijid.2020.06.030

23. S. Funk, M. Salatha, V. A. Jansen, Modelling the influence of human behaviour on the spread of infectious diseases: A review, *J. Royal Soc. Interf.*, **7** (2010), 1247–1256. https://doi.org/10.1098/rsif.2010.0142

24. F. Verelst, L. Willem, P. Beutels, Behavioural change models for infectious disease transmission: a systematic review (2010–2015), *J. Royal Soc. Interf.*, **13** (2016), 20160820. https://doi.org/10.1098/rsif.2016.0820

25. O. Forrest, M. T. Al-arydah, Optimal control strategies for infectious diseases with consideration of behavioral dynamics, *Math. Meth. Appl. Sci.*, **48** (2025), 1362–1380. https://doi.org/10.1002/mma.10388

26. T. Usherwood, Z. LaJoie, V. Srivastava, A model and predictions for COVID-19 considering population behavior and vaccination, *Sci. Rep.*, **11** (2021), 12051. https://doi.org/10.1038/s41598-021-91514-7

27. H. D. Adam, M. Althubyani, S. M. Mirgani, S. Saber, An application of Newton's interpolation polynomials to the zoonotic disease transmission between humans and baboons system based on a time-fractal fractional derivative with a power-law kernel, *AIP Adv.*, **15** (2025), 045217. https://doi.org/10.1063/5.0253869

28. M. Alhazmi, F. M. Dawalbait, A. Aljohani, K. O. Taha, H. D. Adam, S. Saber, Numerical approximation method and Chaos for a chaotic system in sense of Caputo-Fabrizio operator, *Thermal Sci.*, **28** (2024), 5161–5168. https://doi.org/10.2298/TSCI2406161A

29. A. Turab, H. Hilmi, J. L. Guirao, S. Jalil, N. Chorfi, P. O. Mohammed, The Rishi Transform method for solving multi-high order fractional differential equations with constant coefficients, *AIMS Math.*, **9** (2024), 3798–3809. https://doi.org/10.3934/math.2024187

30. K. Diethelm, N. J. Ford, A. D. Freed, Y. Luchko, Algorithms for the fractional calculus: A selection of numerical methods, *Comput. Meth. Appl. Mech. Eng.*, **194** (2005), 743–773. https://doi.org/10.1016/j.cma.2004.06.006

AIMS Press